Neural Processes with Stochastic Attention: Paying More Attention to the Context Dataset

Mingyu Kim, Kyeongryeol Go, Se-Young Yun
KAIST AI
{callingu, kyeongryeol.go, yunseyoung}@kaist.ac.kr

Abstract

Neural processes (NPs) aim to stochastically complete unseen data points based on a given context dataset. NPs essentially leverage a given dataset as a context representation to derive a suitable identifier for a novel task. To improve the prediction accuracy, many variants of NPs have investigated context embedding approaches that generally design novel network architectures and aggregation functions satisfying permutation invariant. In this work, we propose a stochastic attention mechanism for NPs to capture appropriate context information. From the perspective of information theory, we demonstrate that the proposed method encourages context embedding to be differentiated from a target dataset, allowing NPs to consider features in a target dataset and context embedding independently. We observe that the proposed method can appropriately capture context embedding even under noisy data sets and restricted task distributions, where typical NPs suffer from a lack of context embeddings. We empirically show that our approach substantially outperforms conventional NPs in various domains through 1D regression, predator-prey model, and image completion. Moreover, the proposed method is also validated by MovieLens-10k dataset, a real-world problem.

1 Introduction

Neural processes (NPs) have been in the spotlight as they stochastically complete unseen target points considering a given context dataset without huge inference computation [1, 2, 3]. NPs leverage neural networks to derive an identifier suitable for a novel task using context representation, which contains information about given context data points. These methods enable us to handle considerable amounts of data points, such as in image-based applications, that the Gaussian process cannot naively deal with.

Many studies have revealed that the prediction performance relies on the way of context representation [3, 4]. The variants of NPs have mainly investigated on context embedding approaches that generally design novel network architectures and aggregation functions that are permutation invariant. For example, the standard neural processes is developed using MLP layers to embed context set via mean aggregation [1, 2]. Bayesian aggregation satisfying permutation invariance enhanced the prediction accuracy by varying weights for individual context data points [4]. From the prospective of network architectures to increase model capacity, Kim et al. (2019) suggested the way of local representation to consider relations between context dataset and target dataset using deterministic attention mechanism [3, 5]. For robustness under noisy situations, bootstrapping method was proposed to orthogonally apply to variants of NPs [6].

Despite many appealing approaches, one significant drawback of previous NPs is that they still underfit when confronted with noisy situations like real-world problems. This manifests as inaccurate predictions at the locations of the context set as seen in Figure 1a. Additionally, in Figure 1b, the attentive neural process (ANP) fails to capture contextual embeddings because the attention weights

5th Workshop on Meta-Learning at NeurIPS 2021, Sydney, Australia.

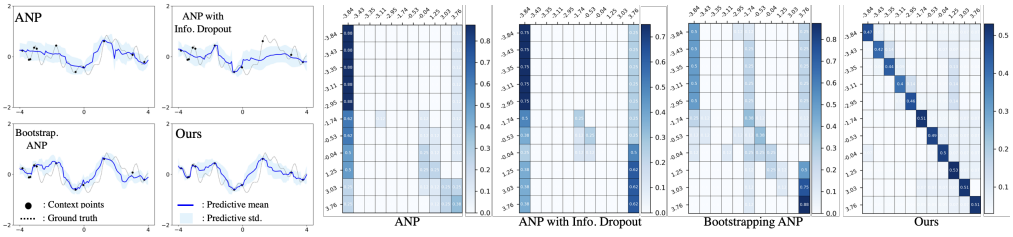

(a) 1D regression predcitions

(b) Heatmaps of asscociated attention weights

Figure 1: Comparison of 1D regression predictions and asscociated attention weights as specified by ANP [3], ANP with Information dropout, Bootstrapping ANP [6] and ours. The training data for 1D regression is fairly noisy. (a) Ours more accurately captures the context datasets and significantly better predicts than baselines. (b) The best pattern for this heat-map is diagonal because all feature values are arranged in ascending order. Among all models, ours comes closet to the ideal. The detailed analysis is shown in Appendix G

of all target points highlight on the lowest value or the maximum value in the context dataset [3]. In the case of the Bootstrapping ANP [6] and ANP with information dropout, the quality of heat-map is slightly improved, but it still falls short of ours. This indicates that the present NPs are unable to properly exploit context embeddings because the noisy situations impair the learning of the context embeddings during meta-training.

To address this issue, we propose a newly designed neural process to fundamentally improve performance by paying more attention to the context dataset. The proposed method expedites a stochastic attention to adequately capture the dependency of the context and target datasets by adjusting stochasticity. We observe that our proposed algorithm properly performs by utilizing contextual information in an intended manner as seen in Figure 1. Thus, this paper clarifies the proposed method as regularized NPs in terms of information theory, explaining that the stochastic attention encourages the context embedding to be differentiated from the target dataset. This differentiated information induces NPs to become appropriate identifiers for target dataset by paying more attention to context representation. To summarize, we make the following contributions:

- We propose the novel neural process that pay more attention to the context dataset. We claims for the first time, using the information theory framework, that critical conditions for contextual embeddings in NPs are independent of target features and close to context datasets.
- Through comprehensive analyses, we illustrate how stochastic local embeddings are crucial for NPs to focus on capturing the dependencies of context and target datasets. Even when context dataset contains noise or is somewhat different from the train dataset, as shown in the bootstrapping NP [6], the proposed method is capable of adapting a novel task while preserving predictive performance. Particularly, this method significantly enhances performance without additional architectures and data augmentation compared to the attentive neural process [3].
- The experimental results show that the proposed model substantially outperforms conventional NPs in typical meta-regression problems. For instance, the proposed method achieves to obtain the state of the art score in the image completion task with the CelebA dataset. Especially, the proposed model maintains performance in the limited task distribution regimes such as the MovieLenz-10k dataset with a small number of users.

2 Background

2.1 Neural Processes

Suppose that we have an observation set $X = \{x_i\}_{i=1}^n$ and a label set $Y = \{y_i\}_{i=1}^n$. NPs [1, 2, 3] are designed to obtain the probabilistic mapping from the observation set to the label set $p(Y|X, X_c, Y_c)$ given a small subset $(X_c, Y_c) = (x_j, y_j)_{j=1}^m$. Basically, it is built upon the neural network with an encoder-decoder architecture where the encoder f_ϕ outputs a task representation by feed-forwarding (X_c, Y_c) through permutation-invariant set encoding [7, 8] and the decoder f_θ models the distribution

of Y (e.g Gaussian case : estimating $\mu,\ \sigma$) using X along with the encoder outputs. Its objective is to maximize the log likelihood over the (unknown) task distribution $p(\mathcal{T})$. All tasks provided by the data generating process are considered as Monte Carlo samples, respectively:

$$\sum_{\mathcal{T}_k \sim p(\mathcal{T})} \log p(Y|X, X_c, Y_c) = \sum_{\mathcal{T}_k \sim p(\mathcal{T})} \sum_{i=1}^{n} \log \mathcal{N}(y_i|\mu_i, \sigma_i) \\ \text{where} \quad (\mu_i, \sigma_i) = f_\theta(x_i, r), \quad r = f_\phi(\{x_j, y_j\}_{j=1}^m) \tag{1}$$

The set encoding architecture differentiates the type of NPs. In the conditional neural process (CNP) [1], the representation r is a deterministic variable such that, by using mean aggregation, the encoder maps the context set into a single deterministic representation $r = {}^1\!/_m \sum_{j=1}^m f_\phi(x_j, y_j)$. The neural process (NP) [2] introduces a probabilistic latent variable z to model functional uncertainty as a stochastic process such that the parameters of output distribution may change according to the sampled value of z. Due to the intractable log-likelihood, a training objective is derived based on variational inference which can be decomposed into two terms, reconstruction term and regularization term:

$$\begin{aligned} \log p(Y|X, X_c, Y_c) &\geq \mathbb{E}_{q_\phi(z|X,Y)} \left[\log \frac{p_\theta(Y|X, r, z) p_\theta(z|X_c, Y_c)}{q_\phi(z|X, Y)} \right] \\ &= \mathbb{E}_{q_\phi(z|X,Y)} \left[\log p_\theta(Y|X, r, z) \right] - \mathrm{KL}(q_\phi(z|X, Y) || p_\theta(z|X_c, Y_c)) \end{aligned} \tag{2}$$

For simplicity, the prior distribution $p_\theta(z|X_c, Y_c)$ is approximated by $q_\phi(z|X_c, Y_c)$. However, as pointed out in the ANP [3], the mean aggregation over the context set is too restrictive to describe the dependencies of the set elements. To enhance the expressiveness of the task representation, the ANP accommodates an attention mechanism [5] into the encoder, which generates the local deterministic representation r_i corresponding to a target data point x_i, and addresses the underfitting issue in NPs. Although additional set encoding methods such as the kernel method and the bayesian aggregation considering task information have been suggested [9, 10, 11, 4], the attentive neural process is mainly considered as the baseline in terms of model versatility.

2.2 Bayesian Attention Module

Consider *m* key-value pairs, packed into a key matrix $K \in \mathbb{R}^{m \times d_k}$ and a value matrix $V \in \mathbb{R}^{m \times d_v}$ and *n* queries packed into $Q \in \mathbb{R}^{n \times d_k}$, where the dimensions of the queries and keys are the same. Attention mechanisms aim to create the appropriate values $O \in \mathbb{R}^{n \times d_v}$ corresponding to Q based on the similarity metric to K, which are typically computed via an alignment score function g such that $\Phi = g(Q, K)$. Then, a softmax function is applied to allow the attention weight $W \in \mathbb{R}^{n \times m}$ to satisfy the simplex constraint so that the output features can be obtained by $O_{i,j} = W_i \cdot V_j$:

$$W_{i,j} = \frac{\exp(\Phi_{i,j})}{\sum_{j=1}^m \exp(\Phi_{i,j})} \tag{3}$$

Note that there are many options for the alignment score function g where a scaled dot-product or a neural network are widely used.

The bayesian attention module [12] considers a stochastic attention weight W. Compared to other stochastic attention methods [13, 14, 15, 16], it requires minimal modification to the deterministic attention mechanism described above so that it is compatible with the existing frameworks, which can be adopted in a straightforward manner. Specifically, un-normalized attention weights $\hat{W}$ such that $W_{i,j} = {}^{\hat{W}_{i,j}}\!/\!_{\sum_{j=1}^m \hat{W}_{i,j}}$ are sampled via the variational distribution $q_\phi(\hat{W}|Q, K)$, which can be trained via amortized variational inference:

$$\log p(O|Q, K, V) \geq \mathbb{E}_{q_\phi(\hat{W}|Q,K)} \left[\log p_\theta(O|V, \hat{W}) \right] - \mathrm{KL}(q_\phi(\hat{W}|Q, K) || p_\theta(\hat{W})) \tag{4}$$

Considering the random variable $\hat{W}$ to be non-negative such that it can satisfy the simplex constraint by normalization, the variational distribution $q_\phi(\hat{W}|Q, K)$ is set to Weibull(k, λ) and the prior distribution $p_\theta(\hat{W})$ is set to Gamma(α, β). This λ can be obtained by the standard attention mechanism, on the other hands, α can be either a learnable parameter or a hyper-parameter depending on that the model follows key-based contextual prior described in the following paragraph. The remaining

variables k and β are regarded as user-defined hyper-parameters. By introducing Euler–Mascheroni constant γ [17, 18], the KL divergence in Equation 4 can be computed in an analytical expression.

$$\text{KL}(\text{Weibull}(k,\lambda)||\text{Gamma}(\alpha,\beta)) = \frac{\gamma\alpha}{k} - \alpha\log k + \beta\lambda\Gamma(1+\frac{1}{k}) - \gamma - 1 - \alpha\log\beta + log\Gamma(\alpha) \quad (5)$$

Samples from Weibull distribution can be obtained using a reparameterization trick exploiting an inverse CDF method: $\lambda(-\log(1-\epsilon))^{\frac{1}{k}},\ \epsilon \sim \text{Uniform}(0,1)$. Note that mean and variance of Weibull(k,λ) are computed as $\lambda\Gamma(1+{}^1\!/_k)$ and $\lambda^2\left[\Gamma(1+{}^2\!/_k) - (\Gamma(1+{}^1\!/_k))^2\right]$. It can be observed that the variance of obtained samples decreases as k increases.

Key-based contextual prior To model the prior distribution of attention weights, key-based contextual prior was proposed. This method allows the neural network to calculate the shape parameter α of the gamma distribution as a prior distribution. This leads to the stabilization of KL divergence between standard attention weights and sampled attention weights, and it prevents overfitting of the attention weights [12]. In this paper, we explain the reason why the key-based context prior is important for capturing an appropriate representation focusing on a context dataset from the prosepective of information theory.

3 Neural Processes with Stochastic Attention

We expect NPs to appropriately represent the context dataset to predict target data points in a novel task. However, if the context dataset has a limited task distribution and noise like real-world problems, conventional NPs tend to sensitively react to this noise and maximize the objective function including irreducible noise. These irreducible noises do not completely correlate with context information, so that this phenomenon derives meaningless set encoding of the context dataset in training phase and hinders adaptation to new tasks. In other words, the output of NPs $p_\theta(y_i|x_i,z,r_i)$ does not depend on (z,r_i).

To preserve the quality of context representation, we propose a method that better utilizes the context dataset by exploiting stochastic attention with the key-based contextual prior to NPs. We show that the proposed method enables to create more precise context encoding by adjusting stochasticity, even in very restricted task distribution regimes.

3.1 Generative Process

As with the attentive neural process [3], the proposed method consists of the two types of encoders and a single decoder architecture. The first encoder embeds (X_c,Y_c) to a global representation z and the second encoder makes a local representation r_i by (x_i,X_c,Y_c). The global representation z serves to represent entire context data points (X_c,Y_c), whereas the local representation r_i is in charge of fine-grained information between target data x_i and context (X_c,Y_c) for predicting the output distribution $p(y_i|x_i,(z,r_i))$. Unlike the ANP, the proposed model considers all intermediate representations (z,r_i) as stochastic variables.

We exploit the Bayesian attention module to create a local representation r_i by the stochastic attention weights w_i with the key-based contextual prior [12]. To use the reparameterization trick for sampling stochastic variables, we draw random noise samples $\epsilon_1 \sim \text{Unif}(0,1), \epsilon_2 \sim \mathcal{N}(0,1)$. First, as mentioned in section 2, the stochastic attention weights $\{w_i\}_{i=1}^N$ are obtained via the inverse CDF of the Weibull distribution with random noise ϵ_1. For amortized variational inference, the prior distribution $q_\phi(\{w\}_{i=1}^N|K(X_c))$ is also derived with the context dataset X_c for implementing key-based contextual prior. Meanwhile, ϵ_2 is used to obtain the global representation z sampled from the normal distribution. The entire scheme is shown in Figure D.2c. As shown in section 2, we can compute all the KL divergences of z and $\{w\}_{i=1}^n$ as closed-form solutions. The decoder follows the standard neural processes $p(y_i|x_i,z,r_i) = \mathcal{N}(y_i|\mu_\phi(x_i,z,r_i),\sigma_\phi^2(x_i,z,r_i))$. We provides Appendix D for implementation details.

3.2 Learning and Inference

Unlike the attentive neural process [3], the proposed method regards all representations z and $W = \{w_i\}_{i=1}^n$ as stochastic variables, so that we clearly drive the objective function according

to amortized variational inference. Based on the objective function of neural process [2], the proposed method adds KL divergence of stochastic attention weight $W = \{w_i\}_{i=1}^n$. Assuming the independence between z and $\{w_i\}_i^n$ such that individual w_i is only dependent on x_i and (X_c, Y_c) as seen in Figure D.2c, the objective function for each task $\mathcal{T}_k$ is presented as follows:

$$\begin{aligned}\mathcal{L}_{\mathcal{T}_k}(\phi,\theta) = \sum_{i=1}^{N}\big[\log p_\theta(y_i|x_i,z,r_i) - \mathrm{KL}\big(q_\phi(w_i|x_i,X_c)|q_\phi(w_i|X_c)\big)\big] \\ - \mathrm{KL}\big(q_\phi(z|X,Y)|q_\phi(z|X_c,Y_c)\big)\end{aligned} \tag{6}$$

Note that (X, Y) follows a task $\mathcal{T}_k$ and each task $\mathcal{T}_k$ is drawn from task distribution $p(\mathcal{T})$. The final objective function is $\mathcal{L}(\phi,\theta) = \mathbb{E}_{\mathcal{T}_k}[\mathcal{L}_{\mathcal{T}_k}(\phi,\theta)]$. From the perspective of amortized variational inference, the prior distributions of $p(z)$ and $p(\{w_i\})_{i=1}^n$ should be defined. With regard to z, we follow the standard neural processes wherein $p(z)$ is defined as $q_\phi(z|\{X_c, Y_c\}$ [2]. In the case of $\{w_i\}_{i=1}^N$, we introduce the strategy of Bayesian attention modules [12]. The prior distribution of $\{w_i\}_{i=1}^N$ defined as a key-based contextual prior, $q_\phi(w_i|X_c)$, not only stabilizes the KL divergence but also activates the representation w_i to pay more attention to the context dataset. In the next section, this objective function can be described in terms of information theory as role of regularization to pursue the original goal of NPs, which is deriving appropriate identifiers for target datasets in novel tasks.

3.3 Discussion of Objective Function from Perspectives of Information Theory

A novel part of the proposed method is the use of the stochastic attention mechanism to more leverage context information, thereby stably capturing the dependency of context and target datasets in noisy and very limited task distributions. In this subsection, based on information theory, we elaborate the goal of NPs and our novel stochastic attention mechanism explained as the regularization of latent variables to pay more attention to context datasets. This enables us to understand semantically latent variables and their requirements. According to subsection 3.2, the objective function is categorized into two terms: a reconstruction $\log p_\theta(y_i|x_i,z,r_i)$ and regularization as two KL Divergences. Suppose that $\{x_i, y_i\}$ is a data point in a target dataset, $\mathcal{D}$ is a given context dataset, latent variables z and r_i are considered as Z, which is defined as the information bottleneck for $\mathcal{D}$, we suggest that maximizing a reconstruction term corresponds to increase $I(y_i, \mathcal{D}|x_i)$ and minimizing two KL Divergence means to decrease $I(Z, x_i|D)$.

First, the mutual information of the target value y_i and the context dataset $\mathcal{D}$ given the input feature x_i, $I(y_i, \mathcal{D}|x_i)$, is the metric to identify that NPs is adapted to a novel task. Suppose $p(y_i|x_i, \mathcal{D})$ is output value of NPs and $p(y_i|x_i) = \mathbb{E}_D\big[p(y_i|x_i, \mathcal{D})\big]$ is output value not conditioned on context dataset $\mathcal{D}$. If NPs completely fail to adapt new tasks using the context dataset $\mathcal{D}$, the suggested metric $I(y_i, \mathcal{D}|x_i)$ goes to 0.

$$I(y_i,\mathcal{D}|x_i) = \mathbb{E}_{y_i,\mathcal{D}}\left[\log\frac{p_\theta(y_i|x_i,\mathcal{D})}{p_\theta(y_i|x_i)}\right] \tag{7}$$

Assumed that target data point $\{x_i, y_i\}$ is sampled from $\mathcal{T}_k$, which is uncontrollable data generating process, the reconstruction term $\sum_{\{x_i,y_i\}}\log p(y_i|x_i, Z)$ can be regarded to $I(y_i; Z|x_i)$ based on information bottleneck theorem; $I(y_i; \mathcal{D}|x_i) \geq I(y_i; Z|x_i)$ holds. A detailed explanation is given in Appendix C. The objective function should be designed to increase $I(y_i, \mathcal{D}|x_i)$ by an appropriate identifier for a novel task considering a context dataset $\mathcal{D}$. However, as mentioned in the previous sections, NPs suffer from irreducible noises and limited task distribution in meta-training. This phenomena means that NPs increase the objective function by learning the way to directly map from x_i to y_i including noises and some features only in meta-training, instead of taking into consideration of the context $\mathcal{D}$. To make latent variables Z capture proper dependencies, we define the regularization accounting for latent variables to pay more attention to the context dataset.

This regularization is the mutual information of latent variable Z and input x_i given context dataset $\mathcal{D}$ to indicates how similar information latent variable Z and target x_i contain. We regard $p(Z|x_i, D)$ as the distribution of latent variables that considers both context dataset D and target x_i, meanwhile $p(Z|D) = \mathbb{E}_{x_i}\big[p(Z|x_i, D)\big]$ as the distribution of latent variables only depending on the context

dataset $\mathcal{D}$. If latent variables Z have totally different information against the target x_i given the context dataset $\mathcal{D}$, It can be $I(Z, x_i|\mathcal{D}) = 0$

$$I(Z, x_i|\mathcal{D}) = \mathbb{E}_{Z,x_i}\left[\log \frac{p(Z|x_i, \mathcal{D})}{p(Z|D)}\right] \tag{8}$$

We bring $I(y_i; \mathcal{D}|x_i) - I(Z, x_i|\mathcal{D})$ to be maximized instead of $I(y_i, \mathcal{D}|x_i)$ so as to model adequately dependency between context and target datasets. By decreasing $I(Z, x_i|\mathcal{D})$ and increasing $I(y_i, \mathcal{D}|x_i)$ in meta-training, we expect that the model learns the way to differentiate Z and x_i and construct an identifier which can further consider Z and x_i together. Note that ϕ is the parameter of the function to transform $\mathcal{D}$ to the information bottleneck Z, and θ is the parameter of the identifier for target data point y_i. We demonstrate that $I(y_i; \mathcal{D}|x_i) - I(Z, x_i|\mathcal{D}) \geq I_{\phi,\theta}(y_i; Z|x_i) - I_\phi(Z, x_i|\mathcal{D})$ if ϕ, θ completely leverage all information about Z and x_i. We assume that neural network architectures can perform an intended manners.

Theorem 1. *Let Z be the representation of the context dataset $\mathcal{D}$ and it follows an information bottleneck. The following equation holds when the latent variable Z can be split into $\{z, w_i\}$ and z is only dependent on $\mathcal{D}$, but w_i is dependent on $\mathcal{D}$ and x_i,*

$$\mathcal{L}_{\mathcal{T}_k}(\phi, \theta) \leq I(y_i; \mathcal{D}|x_i) - I(Z, x_i|\mathcal{D}) \tag{9}$$

where w_i is obtained by the Bayesian attention modules [12], and $\mathcal{L}_{\mathcal{T}_k}$ is defined in Equation 6 and its probabilistic graphical model follows Figure D.2c.

As mentioned, if the neural network architectures ϕ, θ are able to entirely represent to Z and y_i given D and x_i, $\mathcal{L}_{\mathcal{T}_k}(\phi, \theta) = I_{\phi,\theta}(y_i; Z|x_i) - I_\phi(Z; x_i|\mathcal{D})$ ideally holds. In this subsection, we reveal that stochastic attention mechanism satisfy on this regularization. $p(Z|x_i, \mathcal{D})$ is regarded as $q_\phi(w_i|x_i, \{X_c, Y_c\})$ and $p(Z|\mathcal{D})$ is the key-based contextual prior; $q_\phi(w_i|K(X_c))$. Therefore, the stochastic attention mechanism with key contextual prior is considered as this regularization in Equation 8. By Theorem 1, the network parameters ϕ and θ are updated by the gradient of the objective function in Equation 6 semantically improves $I(y_i; \mathcal{D}|x_i) - I(Z, x_i|\mathcal{D})$. Therefore, we present the experimental results in the next section. The empirical results indicate that we can implement a model that can complete unseen data points in novel tasks by fully considering the context representations. The detailed analysis is presented in Appendix G.

4 Experiment

In this section, we describe our experiments to answer three key questions: *1) Are existing regularization methods such as weight decay, importance-weighted ELBO as well as recent methods(Information dropout, Bootstrapping, and Bayesian aggregation) effective to properly create context representations ?; 2) Can the proposed method reliably capture dependencies between target and context datasets even under noisy situations and limited task distributions ?; 3) Is it possible to improve performance via the appropriate representation of the dataset ?*

We choose CNP, NP [1, 2], and ANP [3] as baselines, which are commonly used. For all baselines, we employ weight decay and importance-weighted ELBO that requires several samples against one data point and aggregated by $\log \sum_i \exp \mathcal{L}_k$. Recent regularization methods can be also considered. Information dropout [19, 20], Bayesian aggregation [4] and Bootstrapping [6] are chosen. Bayesian aggregation is used for CNP and NP according to the original paper, meanwhile Information dropout and Bootstrapping are used for the ANP to verify regularization of local representations. As a metric to evaluate the model's predictive performance, we use the likelihood of the target dataset, while the likelihood of the context dataset is considered as a metric to measure the extent to which models can represent a context dataset. Since these metrics are proportional to model performance, a higher value indicates a better performance. In these experiments, we show that the proposed method substantially outperforms various NPs and their regularization methods.

4.1 1D Regression under Noisy Situations

We tested them with samples from various kernel functions (Matern, Periodic inclduing RBF) to identify that models is capable of adaptatation to new tasks. To consider noisy environments, we

Table 1: Results of likelihood values on the synthetic 1D regression experiment. The test samples are drawn from GPs with various kernel functions; All methods are trained on the samples from the RBF GP function. To consider noisy setting, we artificially generate a periodic noise in the training step. **Bold entries** indicates the best results.

	RBF kernel GP(*noises*)		**RBF kernel GP**		**Matern kernel GP**		**Periodic kernel GP**	
	context	target	context	target	context	target	context	target
CNP	0.233±0.036	-0.478±0.034	0.440±0.013	0.026±0.014	0.246±0.021	-0.544±0.024	0.176±0.022	-0.978±0.033
NP	-0.151±0.012	-0.690±0.059	0.107±0.018	-0.177±0.024	-0.235±0.032	-0.918±0.029	-0.400±0.046	-1.321±0.047
ANP	0.228±0.021	-0.603±0.036	0.405±0.0010	-0.097±0.024	0.254±0.006	-0.488±0.014	0.111±0.034	-0.951±0.070
(Weight decay; $\lambda = 0.001$)								
CNP	0.240±0.041	-0.471±0.037	0.460±0.016	0.045±0.020	0.278±0.035	-0.472±0.041	0.185±0.012	-0.970±0.037
NP	-0.153±0.033	-0.709±0.070	0.122±0.026	-0.178±0.036	-0.228±0.034	-0.936±0.026	-0.401±0.047	-1.315±0.072
ANP	0.957±0.015	-0.442±0.030	1.050±0.011	0.053±0.034	1.014±0.009	-0.209±0.036	0.926±0.007	**-0.644±0.027**
(Importance Weighted ELBO; $s = 5$)								
CNP	0.271±0.024	-0.442±0.041	0.478±0.012	0.059±0.029	0.321±0.019	-0.460±0.036	0.231±0.017	-0.957±0.041
NP	-0.155±0.014	-0.633±0.026	0.067±0.016	-0.213±0.030	-0.238±0.015	-0.779±0.018	-0.330±0.008	-1.094±0.088
ANP	0.771±0.012	-0.470±0.034	0.895±0.016	-0.031±0.026	0.800±0.031	-0.324±0.027	0.704±0.026	-0.687±0.039
(Bayesian Aggregation)								
CNP	0.351±0.049	-0.508±0.084	0.575±0.016	0.112±0.025	0.349±0.018	-0.569±0.097	0.278±0.018	-1.026±0.051
NP	-0.406±0.035	-0.723±0.067	-0.201±0.024	-0.389±0.024	-0.450±0.014	-0.837±0.036	-0.537±0.011	-0.877±0.021
(Regularization for local representation)								
ANP *(dropout)*	0.158±0.019	-0.593±0.035	0.372±0.026	-0.163±0.025	0.136±0.020	-0.575± 0.014	0.014±0.017	-0.877±0.036
Bootstrapping ANP	0.754±0.018	-0.407±0.036	0.872±0.009	0.043±0.023	0.788±0.010	-0.303± 0.032	0.711±0.025	-0.717±0.033
Ours	**1.374±0.004**	**-0.337±0.027**	**1.363±0.010**	**0.244±0.026**	**1.365±0.009**	-0.175±0.031	**1.372±0.005**	-0.612±0.029

artificially generate noises into the training dataset. Our model maintains outstanding performance compared to other baselines. In particular, when the test data comes from periodic kernel GP, which is the most different from the RBF GP, the proposed model utilizes context datasets appropriately regardless of the test data sources, whereas other models do not properly use the context data. As shown in Figure 1a, the proposed method captures context points better than other methods, as only it method correctly captures the relationship even under noisy situations.

4.2 Predator-Prey Model and Image Completion

Table 2: Results of likelihood values on the Sim2Real experiment using predator-prey simulation and image completion with the CelebA dataset. In the image completion, there are several experimental cases; The number of context points is in $\{50, 100, 300, 500\}$. We report that likelihood of context points is averaged over all experiment cases and elaborate individual likelihood values of target points. **Bold entries** indicates the best results.

	Sim2Real : Predator-Prey				**Image Completion : CelebA**				
	Simulation		**Real**		**context**	**Target**			
	context	target	context	target		50	100	300	500
CNP	0.395±0.000	0.274±0.000	-2.645±0.085	-3.120±0.245	3.452±0.002	2.662	3.077	3.359	3.414
NP	-0.259±0.004	-0.369±0.002	-2.526±0.030	-2.816±0.088	3.072±0.003	2.483	2.786	2.999	3.042
ANP	1.211±0.001	0.961±0.001	-1.756±0.187	-3.742±0.448	3.100±0.012	2.492	2.806	3.02	3.06
(Weight decay; $\lambda = 0.001$)									
CNP	0.393±0.000	0.265±0.000	-2.661±0.023	-3.049±0.096	2.969±0.014	2.21	2.6	2.866	2.918
NP	-0.069±0.003	-0.185±0.001	-2.571±0.054	-2.914±0.108	2.429±0.008	1.878	2.17	2.368	2.406
ANP	1.520±0.001	1.180±0.002	0.212±0.129	-2.807±0.665	2.832±0.025	2.339	2.611	2.795	2.829
(Importance Weighted ELBO; $s = 5$)									
CNP	0.476±0.000	0.337±0.000	-2.596±0.048	-3.038±0.183	3.474±0.002	2.67	3.091	3.379	3.436
NP	0.055±0.002	-0.067±0.002	-2.514±0.048	-2.760±0.107	3.179±0.023	2.49	2.856	3.112	3.163
ANP	1.004±0.001	0.775±0.001	-1.800±0.203	-3.728±0.486	3.131±0.002	2.477	2.826	3.057	3.101
(Bayesian Aggregation)									
CNP	0.551±0.000	0.429±0.000	-2.654±0.156	-2.952±0.112	3.583±0.013	**2.733**	3.18	3.474	3.53
NP	0.332±0.003	0.192±0.005	-2.489±0.065	-3.009±0.315	3.483±0.032	2.529	3.072	3.4	3.46
(Regularization for local representation)									
ANP *(dropout)*	1.492±0.003	1.134± 0.004	1.068±0.039	-6.215±1.577	3.078±0.006	2.501	2.801	3.005	3.043
Bootstrapping ANP	2.537±0.001	2.166± 0.001	**2.451±0.019**	-3.382±1.288	3.172±0.009	2.453	2.837	3.095	3.145
Ours	**2.711±0.000**	**2.297±0.000**	**2.429±0.031**	-1.766±0.885	**4.119±0.010**	2.653	**3.21**	**3.787**	**3.948**

We apply NPs to a domain shift problem called the predator-prey model, proposed in the ConvCNP [9]. In this experiment, we train models with the simulated data and applied models to predict the real-world data set, Hudson's bay the hare-lynx. Note that the hare-lynx dataset is very noisy, unlike the simulated data. The detailed explanation of datasets is written in Appendix F. We observe that

the proposed method is superior to the other models in both simulated test set and real-world dataset. In particular, all baselines drastically decrease the likelihood values due to noises during the test, while the proposed model preserves the performance because it is robust to noises. See the left side of Table 2. We report the additional experimental result with periodic noises and the graphical explanation is presented in Appendix F.

Second, we conduct the image completion task in which the models generate images under some given pixels. The experiment setting follows the previous experiments [1, 2, 3, 6]. We indicate that the proposed method records the best score as seen in the right side of Table 2. The best baseline records 3.53 with 500 context pixels in Table 2, whereas our method attains 2.653 of likelihood even with 50 context pixels and grows to 3.948 with 500 context pixels. The completed images by ours and baselines are shown in Appendix I.

4.3 Movielens-100k Data

We demonstrate the robustness and effectiveness of our method using a real-world dataset, the MovieLenz dataset, which is commonly used in recommendation systems. This setting has an expensive data collection process that restricts the number of users. In this section, we report how well the proposed method can be generalized to novel tasks using limited tasks during the meta-training.

The proposed model performs better than the other methods. As mentioned in subsection 4.2, it captures the information from the context dataset, while other methods suffer from noise in the data and lack of users in meta-training. The experiment result of comaprison with baselines is reported in Appendix H. To validate use of real applications, we compare with existing studies. According to Movielens-100k benchmarks, the state-of-the-art RMSE score is about 0.890 [22]. As seen in Table 3, the ANP points the comparable result of 0.909, meanwhile the proposed model attains a promising result, 0.895 of the RMSE value. This experiment indicates that the proposed method can reliably adapt to new tasks even if it provides small histories, and we identify again that our model can properly work on noisy situations.

Table 3: Comparison of RMSE scores on u.test in MoveLens-100k

	RMSE
GLocal-K [21]	0.890
GraphRec + Feat [22]	0.897
GraphRec[22]	0.904
GC-MC + Feat[23]	0.905
GC-MC [23]	0.910
ANP (contexts: 10)[3]	0.909
Ours (contexts: 10)	0.895

5 Related Works

The stochastic attention mechanism enables the capturing of complicated dependencies and regularizing weights based on the user's prior knowledge. However, such methods cannot utilize back-propagation because they do not consider the reparameterization trick to draw samples [13, 14, 15, 16]. Recently, the Bayesian attention module suggests that the attention weights are samples from the Weibull distribution whose parameters can be reparameterized, so this method can be stable for training and maintaining good scalability [12].

Since the conditional neural process have been proposed [1, 2], several studies have been conducted to improve the neural processes in various aspects. The attentive neural process modifies the set encoder as an cross-attention mechanism to increase the performance of the predictability and interpretability [3]. Some studies investigate NPs for sequential data [24, 25]. The convolutional network can be used for set encoding to obtain translation-invariant predictions specialized in functional representations with kernel functions [9, 10]. Similar to this study, the Bayesian context aggregation suggests the importance of context information over tasks [4] and the Bootstrapping NPs orthogonally improves the predictive performance under the model-data mismatch [6].

6 Conclusion

In this work, we utilize a stochastic attention mechanism to capture the relationship between the context and target dataset and adjust stochasticity during the training phase for making the model insensitive to noises.

References

[1] Marta Garnelo, Dan Rosenbaum, Christopher Maddison, Tiago Ramalho, David Saxton, Murray Shanahan, Yee Whye Teh, Danilo Rezende, and SM Ali Eslami. Conditional neural processes. In *International Conference on Machine Learning*, pages 1704–1713. PMLR, 2018.

[2] Marta Garnelo, Jonathan Schwarz, Dan Rosenbaum, Fabio Viola, Danilo J Rezende, SM Eslami, and Yee Whye Teh. Neural processes. *arXiv preprint arXiv:1807.01622*, 2018.

[3] Hyunjik Kim, Andriy Mnih, Jonathan Schwarz, Marta Garnelo, Ali Eslami, Dan Rosenbaum, Oriol Vinyals, and Yee Whye Teh. Attentive neural processes. In *International Conference on Learning Representations*, 2019.

[4] Michael Volpp, Fabian Flürenbrock, Lukas Grossberger, Christian Daniel, and Gerhard Neumann. Bayesian context aggregation for neural processes. In *International Conference on Learning Representations*, 2021.

[5] Ashish Vaswani, Noam Shazeer, Niki Parmar, Jakob Uszkoreit, Llion Jones, Aidan N Gomez, Łukasz Kaiser, and Illia Polosukhin. Attention is all you need. In *Advances in neural information processing systems*, pages 5998–6008, 2017.

[6] Juho Lee, Yoonho Lee, Jungtaek Kim, Eunho Yang, Sung Ju Hwang, and Yee Whye Teh. Bootstrapping neural processes. In *Advances in neural information processing systems*, 2020.

[7] Manzil Zaheer, Satwik Kottur, Siamak Ravanbakhsh, Barnabás Póczos, Ruslan R Salakhutdinov, and Alexander J Smola. Deep sets. In *Advances in Neural Information Processing Systems*, 2017.

[8] Harrison Edwards and Amos Storkey. Towards a neural statistician. In *International Conference on Learning Representations*, 2017.

[9] Jonathan Gordon, Wessel P Bruinsma, Andrew YK Foong, James Requeima, Yann Dubois, and Richard E Turner. Convolutional conditional neural processes. In *International Conference on Learning Representations*, 2019.

[10] Andrew Foong, Wessel Bruinsma, Jonathan Gordon, Yann Dubois, James Requeima, and Richard Turner. Meta-learning stationary stochastic process prediction with convolutional neural processes. In H. Larochelle, M. Ranzato, R. Hadsell, M. F. Balcan, and H. Lin, editors, *Advances in Neural Information Processing Systems*, volume 33, pages 8284–8295. Curran Associates, Inc., 2020.

[11] Jin Xu, Jean-Francois Ton, Hyunjik Kim, Adam Kosiorek, and Yee Whye Teh. Metafun: Meta-learning with iterative functional updates. In *International Conference on Machine Learning*, pages 10617–10627. PMLR, 2020.

[12] Xinjie Fan, Shujian Zhang, Bo Chen, and Mingyuan Zhou. Bayesian attention modules. In H. Larochelle, M. Ranzato, R. Hadsell, M. F. Balcan, and H. Lin, editors, *Advances in Neural Information Processing Systems*, volume 33, pages 16362–16376. Curran Associates, Inc., 2020.

[13] Shiv Shankar and Sunita Sarawagi. Posterior attention models for sequence to sequence learning. In *International Conference on Learning Representations*, 2018.

[14] Dieterich Lawson, Chung-Cheng Chiu, George Tucker, Colin Raffel, Kevin Swersky, and Navdeep Jaitly. Learning hard alignments with variational inference. In *2018 IEEE International Conference on Acoustics, Speech and Signal Processing (ICASSP)*, pages 5799–5803. IEEE, 2018.

[15] Hareesh Bahuleyan, Lili Mou, Olga Vechtomova, and Pascal Poupart. Variational attention for sequence-to-sequence models. In *Proceedings of the 27th International Conference on Computational Linguistics*, pages 1672–1682, 2018.

[16] Yuntian Deng, Yoon Kim, Justin Chiu, Demi Guo, and Alexander Rush. Latent alignment and variational attention. In S. Bengio, H. Wallach, H. Larochelle, K. Grauman, N. Cesa-Bianchi, and R. Garnett, editors, *Advances in Neural Information Processing Systems*, volume 31. Curran Associates, Inc., 2018.

[17] Hao Zhang, Bo Chen, Dandan Guo, and Mingyuan Zhou. Whai: Weibull hybrid autoencoding inference for deep topic modeling. In *International Conference on Learning Representations*, 2018.

[18] Christian Bauckhage. Computing the kullback-leibler divergence between two generalized gamma distributions. *arXiv preprint arXiv:1401.6853*, 2014.

[19] Durk P Kingma, Tim Salimans, and Max Welling. Variational dropout and the local reparameterization trick. In *Advances in neural information processing systems*, pages 2575–2583, 2015.

[20] Alessandro Achille and Stefano Soatto. Information dropout: Learning optimal representations through noisy computation. *IEEE transactions on pattern analysis and machine intelligence*, 40(12):2897–2905, 2018.

[21] Soyeon Caren Han, Taejun Lim, Siqu Long, Bernd Burgstaller, and Josiah Poon. Glocal-k: Global and local kernels for recommender systems. *arXiv preprint arXiv:2108.12184*, 2021.

[22] Ahmed Rashed, Josif Grabocka, and Lars Schmidt-Thieme. Attribute-aware non-linear co-embeddings of graph features. In *Proceedings of the 13th ACM Conference on Recommender Systems*, pages 314–321, 2019.

[23] Rianne van den Berg, Thomas N Kipf, and Max Welling. Graph convolutional matrix completion. *arXiv preprint arXiv:1706.02263*, 2017.

[24] Jaesik Yoon, Gautam Singh, and Sungjin Ahn. Robustifying sequential neural processes. In *International Conference on Machine Learning*, pages 10861–10870. PMLR, 2020.

[25] Gautam Singh, Jaesik Yoon, Youngsung Son, and Sungjin Ahn. Sequential neural processes. In *Advances in Neural Information Processing Systems*, volume 32. Curran Associates, Inc., 2019.

[26] Edney W Stacy et al. A generalization of the gamma distribution. *The Annals of mathematical statistics*, 33(3):1187–1192, 1962.

[27] Yuri Burda, Roger B Grosse, and Ruslan Salakhutdinov. Importance weighted autoencoders. In *ICLR (Poster)*, 2016.

[28] Diederik P Kingma and Jimmy Ba. Adam: A method for stochastic optimization. In *International Conference on Learning Representations*, 2015.

[29] Janarthanan Rajendran, Alexander Irpan, and Eric Jang. Meta-learning requires meta-augmentation. In *Advances in Neural Information Processing Systems*, volume 33, 2020.

[30] Darren J Wilkinson. *Stochastic modelling for systems biology*. Chapman and Hall/CRC, 2018.

[31] Alexandre Galashov, Jonathan Schwarz, Hyunjik Kim, Marta Garnelo, David Saxton, Pushmeet Kohli, SM Eslami, and Yee Whye Teh. Meta-learning surrogate models for sequential decision making. *arXiv preprint arXiv:1903.11907*, 2019.

A Closed Form Solution for The KL Divergence Between Weibull and Gamma Distribution

The generalized gamma distribution contains both Weibull and gamma distribution as special cases. We are concerned with the three-parameter version of generalized gamma distribution introduced in Stacy [26]. Its parameters can be categorized into one scale parameter a and two shape parameters d and p. Its probability density function is defined for $x \in [0, \infty)$ and given by

$$f(x|a, d, p) = \frac{p}{a^d} \frac{x^{d-1}}{\Gamma(d/p)} \exp\left[-(\frac{x}{a})^p\right] \tag{A.1}$$

where $\Gamma(\cdot)$ is the gamma function, and parameters $a, d, p > 0$. For $d = p$, it corresponds to the Weibull distribution, and if $p = 1$, it becomes the gamma distribution. Bauckhage [18] derives a closed form solution for the kullback-leibler divergence between two generalized gamma distribution as follow.

$$\begin{aligned} \mathrm{KL}(f_1|f_2) := & \int_0^\infty f_1(x|a_1, d_1, p_1) \log \frac{f_1(x|a_1, d_1, p_1)}{f_2(x|a_2, d_2, p_2)} dx \\ = & \log\left(\frac{p_1 a_2^{p_2} \Gamma(d_2/p_2)}{p_2 a_1^{p_1} \Gamma(d_1/p_1)}\right) + \left[\frac{\psi(d_1/p_1)}{p_1} + \log a_1\right](d_1 - d_2) \\ & + \frac{\Gamma(\frac{d_1+p_2}{p_1})}{\Gamma(\frac{d_1}{p_1})} \left(\frac{a_1}{a_2}\right)^{p_2} - \frac{d_1}{p_1} \end{aligned} \tag{A.2}$$

where f_1, f_2 are the generalized gamma distributions, and $\psi(\cdot)$ is digamma function. The Weiull distribution with scale parameter λ and shape parameter K coincides with the generalized gamma distribution $a = \lambda$ and $d, p = K$. For gamma distribution with scale parameter β and shape parameter α, it becomes the generalized gamma distribution $a = 1/\beta$, $d = \alpha$ and $p = 1$. The KL divergence between the Weibull distribution (λ, k) and the gamma distribution (α, β) amounts to

$$\begin{aligned} \mathrm{KL}(f_1|f_2) = & \log k - \alpha \log \beta + \log \Gamma(\alpha) \\ & + \psi(1) - \frac{\alpha}{ks}\psi(1) - \alpha \log \lambda + \lambda\beta\Gamma(1 + 1/K) - 1 \end{aligned} \tag{A.3}$$

We introduce $\psi(1) = -\gamma \approx 0.5772$ as Euler constant. Finally, we obtain Equation 5

$$\begin{aligned} \mathrm{KL}(\text{Weibull}(k, \lambda)||\text{Gamma}(\alpha, \beta)) = & \frac{\gamma\alpha}{k} - \alpha \log \lambda + \log k + \beta\lambda\Gamma\left(1 + \frac{1}{k}\right) \\ & - \gamma - 1 - \alpha \log \beta + \log \Gamma(\alpha) \end{aligned} \tag{A.4}$$

B ELBO Derivations

In this section, we derive the objective function in the manuscript of this paper. Without loss of generality, target dataset $\{X, Y\} = \{x_i, y_i\}_{i=1}^{N}$ and context dataset $\mathcal{D} = (X_c, Y_c) = \{x_i, y_i\}_{j=1}^{M}$ such that $N \gg M$. Let the log-likelihood of target data points in a task T_k be $\log p(Y|X, D)$. We begin to maximizing the log-likelihood of target data points based on context dataset and representations. We suppose that it follows the graphical model in Figure D.2c

$$\log p(Y|X, D) = \log \int p(Y, Z|X, D) dz \tag{B.5}$$

$$= \log \int p(Y, Z|X, D) \frac{q(Z|X, D)}{q(Z|X, D)} dz \tag{B.6}$$

$$= \log \int \frac{p(Y, Z|X, D)}{q(Z|X, D)} q(Z|X, D) dz \tag{B.7}$$

$$= \log \int \prod_{i=1} \frac{p(y_i|x_i, Z_i)}{q(Z_i|x_i, \mathcal{D})} p(z_i|x_i, \mathcal{D}) q(z_i|x_i, \mathcal{D}) dz \tag{B.8}$$

$$= \log \mathbb{E}_{q(z)} \big[\prod_{i=1} \frac{p(y_i|x_i, Z_i)}{q(Z_i|x_i, \mathcal{D})} p(z_i|x_i, \mathcal{D}) \big] \tag{B.9}$$

Applying Jensen's inequality to

$$\log p(Y|X, D) \geq \mathbb{E}_{q(z)} \Big[\log \prod_{i=1} \frac{p(y_i|x_i, Z_i) p(Z_i|x_i, \mathcal{D})}{q(z_i|x_i, \mathcal{D})} \Big] \tag{B.10}$$

$$\geq \mathbb{E}_{q(z)} \Big[\sum_{i=1} \log p_\theta(y_i|x_i, Z_i) - \log \frac{q(Z_i|x_i, \mathcal{D})}{p(Z_i|x_i, \mathcal{D})} \Big] \tag{B.11}$$

From $Z_i = \{z, w_i\}$ in Figure D.2c, we define z is dependent on context dataset $\mathcal{D}$ and w_i is dependent on target x_i and context dataset $\mathcal{D}$

$$\log p(Y|X, D) \geq \mathbb{E}_{q(z)} \Big[\sum_{i=1} \log p_\theta(y_i|x_i, Z_i) - \log \frac{q(w_i|x_i, \mathcal{D})}{p(w_i|x_i, \mathcal{D})} - \log \frac{q(z|\mathcal{D})}{p(z|\mathcal{D})} \Big] \tag{B.12}$$

We assume that $p(w_i|x_i, \mathcal{D}) \approx q_{\phi_{1_2}}(w_i|K(X_c))$ by regularization of latent variables to pay attention on context dataset. It also follows the strategy of the standard neural processes : posterior distribution of z is $q_{\phi_2}(w_i|\{X_t, Y_t\})$ and prior distribution of z is $q_{\phi_2}(w_i|\{X_c, Y_c\})$. Thereby, we show that ELBO become the objective function of the proposed method in Equation 6.

$$\log p(Y|X, D) \geq \mathbb{E}_{q(z)} \Big[\sum_{i=1} \log p_\theta(y_i|x_i, Z_i) - \log \frac{q_{\phi_{1_1}}(w_i|x_i, \mathcal{D})}{q_{1_2}(w_i|, K(X_c))} - \log \frac{q_{\phi_2}(z|\{X_t, Y_t\})}{q_{\phi_2}(z|\{X_c, Y_c\})} \Big] = \mathcal{L}_{\mathcal{T}_k} \tag{B.13}$$

C Proof of Theorem 1

We present that $I(y_i;\mathcal{D}|x_i)$ has relation to the objective function of the proposed method. Suppose that Z is information bottleneck for $\mathcal{D}$ and all variables follow the graphical models Figure D.2c. As described in Equation 7, the mutual information $I(y_i,\mathcal{D}|x_i)$ is to measure dependency of y_i and context dataset $\mathcal{D}$. We should maximize this information to generalize the novel task. For simplicity, we set all latent variables as information bottleneck Z for the context dataset $\mathcal{D}$. Note that $Z=(\{w_i\}_{i=1}^n, z)$ is information bottleneck corresponding to context representations in NPs, where $W=\{w_i,\dots,w_n\}$ is an attention weights and $X,Y=\{(x_1,y_1),\dots,(x_n,y_n)\}$ is respectively data points in the target data set. ϕ is regarded as the parameter of the function to transform $\mathcal{D}$ to the information bottleneck Z and θ is the parameter of the identifier for target data point y_i. By information bottleneck theorem, Equation C.14 holds.

$$I(y_i;\mathcal{D}|x_i) \geq I_{\phi,\theta}(y_i;Z|x_i) = -H_{\phi,\theta}(y|x_i,Z) + H(y|x_i) \tag{C.14}$$

The target data point $\{x_i,y_i\}$ is drawn by the data generating process $\mathcal{T}_k \sim p(\mathcal{T})$, so that $H(y|x_i)$ can be regarded as a constant value due to uncontrollable factors. As a result, $-H_{\phi,\theta}(y|x_i,Z)$ is written as

$$-H_{\phi,\theta}(y_i|x_i,Z) = \mathbb{E}_{(x,y)}\big[-\log p_\theta(y_i|x_i,Z)\big] \tag{C.15}$$

We employ $\sum_{\{x_i,y_i\}} \log p_\theta(y_i|x_i,Z_\phi)$, which is unbiased estimate for $-H_{\phi,\theta}(y_i|x_i,Z)$ based on Monte Carlo sampling. Given that the concrete information bottleneck Z is given, we expect that the Z allows us to generalize a novel task $\{x_i,y_i\}$ by enhancing $\sum_{\{x_i,y_i\}} \log p_\theta(y_i|x_i,Z_\phi)$. However, in practice, Z induced by neural networks is more likely to memorize the training dataset including irreducible noises when the number of tasks is insufficient. The conventional methods accomplished maximizing $\sum_{\{x_i,y_i\}} \log p_\theta(y_i|x_i,Z_\phi)$ by simply finding the relation between y_i and x_i only in the training dataset. It means that the information in representation Z becomes increasingly identical to the information in x_i in the meta training dataset. It does not satisfy the condition of information bottleneck for the context dataset $\mathcal{D}$.

To avoid this issue, we introduce $I(Z,x_i|\mathcal{D})$ as a regularization. By reducing dependencies of Z and x_i, we can make the information bottleneck Z focus on $\mathcal{D}$. It means that as $p(Z|x_i,\mathcal{D})$ and $P(Z|\mathcal{D})$ get closer, the target input x_i less influences Z, but $\mathcal{D}$ has a high correlation with Z. In other words, minimizing $I(Z,x_i|\mathcal{D})$ is to make Z and target x_i more independent given context dataset $\mathcal{D}$. It encourages latent variables $Z=(w_i,z)$ to pay more attention to context dataset $\mathcal{D}$

$$\begin{aligned} I(Z,x_i|\mathcal{D}) &= \mathbb{E}_{x_i}\left[\mathbb{E}_{Z_i}\left[\mathrm{KL}(q(Z_i|x_i,\mathcal{D})||q(Z_i||\mathcal{D}))\right]\right] \\ &= \mathbb{E}_{x_i}\Big[\mathbb{E}_{w_i}\left[\mathrm{KL}(q(w_i|x_i,\mathcal{D})||q(w_i|\mathcal{D}))\right] + \mathbb{E}_z\left[\mathrm{KL}(q(z|x_i,\mathcal{D})||q(z|\mathcal{D}))\right]\Big] \end{aligned} \tag{C.16}$$

where, the $q(w_i|x_i,\mathcal{D})$ follows the Weibull distribution and $q(w_i|\mathcal{D})$ follows the gamma distribution. In this study, $q(w_i|x_i,\mathcal{D})$ can be modeled as the stochastic attention weights and $q(w_i|\mathcal{D})$ can be modeled as the key-based contextual prior $q_\phi(w_i|K)$. We can factorize all latent variables because the attention weight w_i does not have a dependency on data points except for the specific data point $\{x_i,y_i\}$. We denote that w_i has conditional independence over $\{w_j\}_{i\neq j}$ given x_i. For the global representation; z, to follow objective function of neural processes, we assume $q(z|x_i,\mathcal{D}) = q_\phi(z|X,Y)$ and $q_\phi(z|\mathcal{D}) = q(z|\mathcal{D})$. As mentioned in section 3, we suppose that the global representation z follows normal distribution. Therefore, we derive the regularization term $I(Z,x_t|\mathcal{D})$ have relation to KL Divergence terms in our loss function. From this fact, we recognize KL Divergence terms in our objective function helps latent variables give attention on context dataset.

To summarize the mutual information between y_i and $\mathcal{D}$, and the newly designed regularization, we found that

$$\begin{aligned} I(y_i;\mathcal{D}|x_i) &\geq I_{\phi,\theta}(y_i;Z|x_i) - I(Z,x_i|\mathcal{D}) \\ &\geq -H_{\phi,\theta}(y|x_i,Z) - I(Z,x_i|\mathcal{D}) + \text{Constant} \end{aligned} \tag{C.17}$$

Based on the graphical models in Figure D.2c and assumptions of representations z and w_i, we identify that this equation has relation to our objective function $\mathcal{L}_{\mathcal{T}_k}$

$$\begin{aligned} I_{\phi,\theta}(y_i; Z|x_i) - I(Z, x_i|\mathcal{D}) = & \sum_{\{x_i,y_i\}} \log p_\theta(y_i|x_i, Z_\phi) - \mathbb{E}_z \left[\text{KL}(q_\phi(z|X,Y)|q_\phi(z|X_c,Y_c))\right] \\ & - \mathbb{E}_W \left[\text{KL}(q_\phi(W|X,\mathcal{D})|q_\phi(W|K(X_c)\right] + \text{Constant} \\ = & \ \mathcal{L}_{\mathcal{T}_k} + \text{Constant} \end{aligned} \tag{C.18}$$

Finally, we can derive Theorem 1 as below

$$\mathcal{L}_{\mathcal{T}_k}(\phi, \theta) \leq I(y_i; \mathcal{D}|x_i) - I(Z, x_i|\mathcal{D}) \tag{C.19}$$

From Equation C.19, the gradients of ϕ and θ with respect to $\mathcal{L}_{\mathcal{T}_k}$ can be regarded as the direction of increasing $I(y_i; \mathcal{D}|x_i) - I(Z, x_i|\mathcal{D})$, where, $\mathcal{L}_{\mathcal{T}_k}$ is defined as the target likelihood and KL divergence of z and $\{w_i\}_{i=1}^n$ in a single task.

$$\begin{aligned} \mathcal{L}_{\mathcal{T}_k}(\phi, \theta) = \sum_{i=1}^{N} & \big[\log p_\theta(y_i|x_i, z, r_i) - \text{KL}\big(q_\phi(w_i|x_i, \mathcal{D})|q_\phi(w_i|X_\mathcal{D})\big)\big] \\ & - \text{KL}\big(q_\phi(z|X,Y)|q_\phi(z|\mathcal{D})\big) \end{aligned} \tag{C.20}$$

where $X_\mathcal{D}$ is input features in the context dataset and $q_\phi(w_i|X_\mathcal{D})$ follows key-based contextual prior as described in section 3.

D Implement Details

We referred to most of the architectures from the paper[3] and their released source code[1]. The information dropout and importance weighted ELBO were respectively borrowed from these papers[19, 27][2][3]. The stochastic attention can be implemented based on Bayesian attention modules[12][4]. We migrated and revised all codes to meet our purpose. In this chapter, we follow the notation of this paper [6].

D.1 (Attentive) Neural Process

MLP Encoder We suppose that multi-layers modules(MLP) have the structure as Equation D.21, where l is the number of layers, d_{in} is the dimension of input features, d_{hidden} is the dimension of hidden units and d_{out} is the dimension of outputs.

$$\begin{aligned}\text{MLP}(l, d_{\text{in}}, d_{\text{hidden}}, d_{\text{out}}) &= \text{Linear}(d_{\text{hidden}}, d_{\text{out}}) \\ &= \circ \underbrace{(\text{ReLU} \circ \text{Linear}(d_{\text{hidden}}, d_{\text{hidden}}) \cdots)}_{l-2} \\ &\quad \circ (\text{ReLU} \circ \text{Linear}(d_{\text{in}}, d_{\text{hidden}}))\end{aligned} \tag{D.21}$$

The variants of neural processes have two types of MLP encoders: The deterministic path is used in the conditional neural process [1], and the stochastic path is employed in the neural process [2], attentive neural process [3] and ours. The deterministic path is to aggregate all hidden units by the MLP encoder.

$$\begin{aligned}h &= \frac{1}{|c|}\sum_{j\in c} \text{MLP}(l_{\text{pre}}, d_x + d_y, d_h, d_h)([x_j, y_j]) \\ r &= \text{MLP}(l_{\text{post}}, d_h, d_h)(h)\end{aligned} \tag{D.22}$$

Instead, the stochastic path is to aggregate all hidden units and then feed-forward a single network to generate μ_{ϕ_1} and σ_{ϕ_1}. We obtain the stochastic path r via the reparameterization trick.

$$\begin{aligned}h &= \frac{1}{|c|}\sum_{j\in c} \text{MLP}(l_{\text{pre}}, d_x + d_y, d_h, d_h)([x_j, y_j]) \\ \mu_{\phi_1}, \sigma_{\phi_1} &= \text{MLP}(l_{\text{post}}, d_h, d_h)(h) \\ r &= \mu_{\phi_1} + \epsilon_2 * \sigma_{\phi_1}\end{aligned} \tag{D.23}$$

Attention encoder We introduce cross-attention to describe the dependency of context and target dataset. Let MHA be a multi-head attention [5] computed as follows :

$$\begin{aligned}Q' &= \{\text{Linear}(d_q, d_h)(q)\}_{q\in Q} \\ K' &= \{\text{Linear}(d_k, d_h)(k)\}_{k\in K} \\ V' &= \{\text{Linear}(d_v, d_h)(v)\}_{v\in V} \\ H &= \text{softmax}(Q'K'/\sqrt{d_h})V' \\ \text{MHA}(Q, K, V) &= \text{LayerNorm}(H)\end{aligned} \tag{D.24}$$

Where, $\{d_q, d_k, d_v\}$ are respectively the dimensions of query, key and value components. The LayerNorm is the layer normalization in terms of heads.

MLP Decoder The architecture of MLP decoder is similar to the stochastic encoder. In case of CNP [1] and NP [2], this decoder transforms all representation z and the input feature $\{x_i\}_{i\in T}$ to target distribution, the normal distribution, $\{\mu_i, \sigma_i\}_{i\in T}$.

$$(\mu_y, \sigma_y) = \text{MLP}(l_{\text{dec}}, d_x + d_h, d_h, 2d_y)([z, r_i, x_i]) \tag{D.25}$$

[1] https://github.com/deepmind/neural-processes
[2] https://github.com/kefirski/variational_dropout
[3] https://github.com/JohanYe/IWAE-pytorch
[4] https://github.com/zhougroup/BAM

Meanwhile, in case of attentive neural process [3] and ours, the inputs of this decoder are the global representation z, local representation $\{r_i\}_{i\in T}$ and the input feature $\{x_i\}_{i\in T}$.

$$(\mu_y, \sigma_y) = \text{MLP}(l_{\text{dec}}, d_x + d_h + d_h, d_h, 2d_y)([z, r_i, x_i]) \tag{D.26}$$

The detailed information of each architecture is described in Table D.1.

Table D.1: Architecture details and hyperparameters for the neural processes. Attention indicates variants of attentive neural processes used. Encoder and decoder indicate the MLP network sizes used.

Models	MLP Encoder	Attention Encoder	MLP Decoder	Weight decay	MC samples	Rep. by functions	Information dropout	Stochastic attention
CNP	3×128	-	3×128	0.001 (for *CNP_WD*)	5 (*IWAE*)	-	-	-
NP	3×128	-	3×128	0.001 (for *NP_WD*)	5 (*IWAE*)	-	-	-
CNP_BA	3×128	-	3×128	-	5	-	-	-
NP_BA	3×128	-	3×128	-	5	-	-	-
ANP	3×128	Multi-heads : 8	3×128	0.001 (for *ANP_WD*)	5 (*IWAE*)	-	-	-
ANP *(dropout)*	3×128	Multi-heads : 8	3×128	-	-	-	✓	-
Bootstrapping ANP	3×128	Multi-heads : 8	3×128	-	5	-	-	-
Ours	3×128	Multi-heads : 8	3×128	-	-	-	-	✓

Table D.2: The number of network parameters required for all experimental cases.

Models	**1D regression**	**Sim2Real**	**MovieLenz-100k**	**Image Completion**
CNP	99,842	100,228	110,850	1,583,110
NP	116,354	116,740	127,362	1,845,766
CNP_BA	116,354	116,740	127,362	1,845,766
NP_BA	116,354	116,740	127,362	1,845,766
ANP	595,714	596,228	617,730	9,466,886
ANP *(dropout)*	628,610	629,124	650,626	9,991,686
Bootstrapping ANP	628,610	629,124	650,626	9,991,686
Ours	597,015	597,529	619,031	9,472,027

Table D.3: Time required for inference in all experiment cases. (*1 epoch*).

Models	**1D regression**	**Sim2Real**	**MovieLenz-10k**	**Image Completion : CelebA**			
				50	100	300	500
CNP	0.860	0.896	0.829	1.274	1.321	1.390	1.390
NP	1.411	1.422	1.356	1.975	1.990	1.959	2.081
CNP_BA	1.143	1.215	2.149	1.629	1.644	2.091	2.221
NP_BA	1.930	2.003	3.198	3.074	3.106	3.709	4.017
ANP	2.442	2.500	2.222	5.294	5.710	9.010	11.740
ANP *(dropout)*	3.283	3.328	2.967	5.961	6.376	9.926	12.710
Bootstrapping ANP	6.474	6.968	6.250	26.186	30.012	60.619	88.332
Ours	3.152	5.848	3.121	11.350	19.217	57.898	95.031

Unit : second

In this paper, we set the dimension of all latent variables as 128, namely $d_h = 128$. The number of heads in multi-head attention is 8, which is the same as the original paper of attentive neural processes [3]. For all models and all experiments, we use the Adam optimizer [28] with the learning rate 0.001, and we set the number of update steps as 200000.

For training and evalation, we used AMD Ryzen 2950X(16-cores), RAM 64GB and RTX2080Ti. The 1D regressions has a batch size of 1 and a total of 160 batches. The Sim2Real configures the batch size to be 10 and the total number of batches to be 16. The MovieLenz-100k has a batch size of 1 and the number of batches to be 459. The image completion task consists of 227 batches and its size is 4.

D.2 Model architecture

We graphically show the architecture of the proposed method in Figure D.1. This model has two types of encoder as attentive neural process [3]. The encoder parameters ϕ consists of ϕ_1, ϕ_2. The

ϕ_1 is responsible for the local representation r_i and the ϕ_2 is responsible for global representation z. The encoder of global representation is same as neural process [2], however, the encoder of local representation is different from the standard cross attention [5]. After obtaining standard attention weight $w_{standard}$, we introduce reparameterization trick for w_i, which follows the Weiubll distribution [12]. The important thing is that the key conceptual prior can be made by $\text{MLP}_{\phi_{1_3}}(\{x_j\}_{j \in C})$. The decoder is the same as the attentive neural process [3].

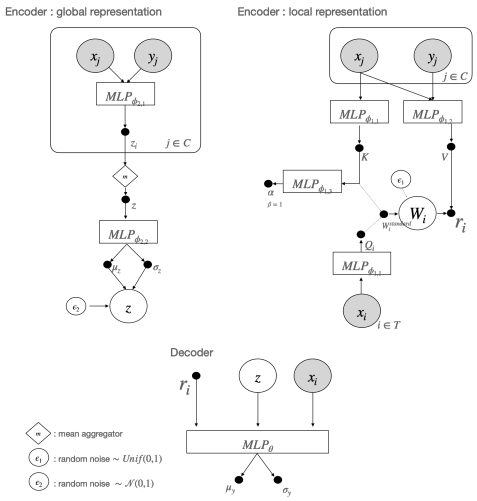

Figure D.1: Model Architectures of the proposed method

D.3 Algorithm

The proposed method requires hyper-parameters k and β for reparameterization of the Weibull distribution and KL divergence between the Weibull and the gamma distribution. We conduct the grid searches for k to find the best value. We identify that the proposed method with $k = 300$ adequately captures the dependency and generates noises to avoid memorization for all experiments. In the case of β, we follow the setting of the Bayesian attention module [12]. We suggest the entire procedure of our algorithm as follows:

D.4 Comparison of probabilistic graphical models for variants of NPs

We describe NPs with probabilistic graphical models to differentiate the variants of NPs. The Neural process employs mean aggregate function and reparameterization trick to obtain a global context representation z [2]. This model follows Figure D.2a. The Attentive neural process expedites the multi-head cross attention to obtain local representation r_i with global context representation z. We show that the graphical model for ANP is the middle of Figure D.2, all variables in the attention mechanism are regarded as the determinstic variable.

In this work, we design that all latent variables contain stochasticity and achieves by the reparameterization trick. By Bayesian attention module, we present our graphical model as shown in Figure D.2c

Algorithm 1: Neural Process with stochastic attention

Input: Task distribution $p(\mathcal{T})$, the shape parameters of weibull distribution and gamma distribution : $k = 300$(Image completion task : $k = 100$), $\beta = 1$, Stepsize : γ
output: encoder parameters : $\phi = \{\phi_1, \phi_2\}$, decoder parameters : θ
Initialization : ϕ and θ randomly;
while *not converged* **do**
  Sample tasks $\{\mathcal{T}_k\}_{k=1}^{K}$ from $p(\mathcal{T})$
  for *all* $\mathcal{T}_k \ni \{\mathcal{T}\}$ **do**
    Sample context dataset $(X_c, Y_c) = \{x_j, y_j\}_{j=1}^{M}$ and target dataset $(X_t, Y_t) = \{x_i, y_i\}_{i=1}^{N}$ from the task $\mathcal{T}_k$
    Sample random noises $\epsilon_1 \sim \text{Unif}(0,1)$ and $\epsilon_2 \sim \mathcal{N}(0,1)$
1 **Local representation** $\{r_i\}_{i=1}^{N}$**:**
      Q, K, V $\leftarrow f_{\phi_1}(X_t, (X_c, Y_c))$
      $w_{\text{standard}} \leftarrow \text{Softmax}(QK^T/\sqrt{d_k})$
      (Reprameterization sampling of weibull distribution for W)
        $\lambda \leftarrow w_{\text{standard}} * \Gamma(1 + 1/k)$
        $W = \{w_1, \cdots, w_n\} \leftarrow \lambda(-\log(1-\epsilon_1))^{1/k}$
        $W = \{w_1, \cdots, w_n\} \leftarrow \{\frac{w_i}{\sum W_i}, \cdots, \frac{w_n}{\sum W_i}\}$
      (Parameters of the prior distribution for W)
        $\alpha \leftarrow f_{\phi_1}(K)$
      $\{r_i\}_{i=1}^{N} \leftarrow \{w_i V, \cdots, w_n V\}$
2 **Global representation** z **:**
      $\mu_{\phi_1}, \sigma_{\phi_1} \leftarrow \text{Aggregator}(f_{\phi_2}(\{x_j, y_j\}_{j=1}^{M}))$
      (Reprameterization sampling of normal distribution for z)
        $z = \mu_{\phi_2} + \epsilon_2 * \mu_{\phi_2}$
3 **Decode** $p(Y_t | X_t, z, \{r_i\}_{i=1}^{N})$ **:**
      $\mu_y, \sigma_y \leftarrow (f_\theta(X_t, z, \{r_i\}_{i=1}^{N}))$
4 **Evaluation loss :**
      $\mathcal{L}_{\phi,\theta}{}^{\mathcal{T}_k} = \sum_{i=1}^{N} \big[\log p_\theta(y_i|\mu_{y,i}, \sigma_{y,i}) - \text{KL}\big(q_{\phi_2}(z|\{X_t, Y_t\})|q_{\phi_2}(z|\{X_c, Y_c\})\big) - \text{KL}\big(q_{\phi_1}(w_i|x_i, X_c)|q_{\phi_1}(w_i|X_c)\big)\big]$
  end
  Update $\phi \leftarrow \phi + \gamma \nabla_\phi \frac{1}{|\mathcal{T}|} \sum_{\mathcal{T}_k} \mathcal{L}^{\mathcal{T}_k}$
  Update $\theta \leftarrow \theta + \gamma \nabla_\phi \frac{1}{|\mathcal{T}|} \sum_{\mathcal{T}_k} \mathcal{L}^{\mathcal{T}_k}$
end

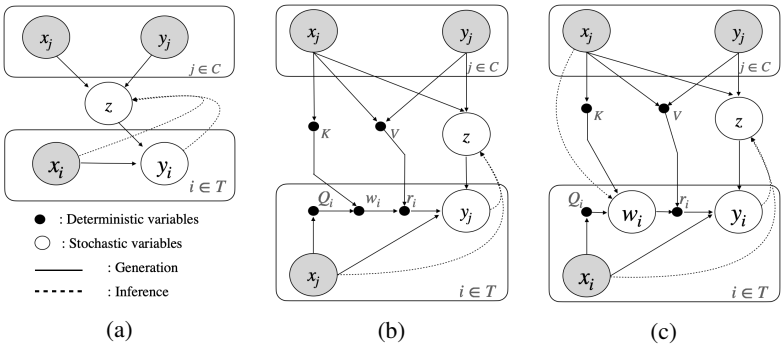

Figure D.2: Comparison of graphical models; (a) Neural process [2], (b) Attentive neural process [3] and (c) Proposed method

E 1D regressions

For the synthetic 1D regression experiment, we set $d_x = 1, d_y = 1$. The number of layers in encoder and decoder in all baselines is respectively $l_{enc} = \{l_{pre} = 3, l_{post} = 1\} = 4$ and $l_{dec} = 3$. We set the dimension of latent variable as $d_h = 128$.

When it comes to data generation process, the training data is generated from the Gaussian process with RBF kernel. For each task, we randomly generate $x \sim Unif(-2, 2)$ and then y is the function value by the Gaussian process with RBF kernel, $k(x, x') = s^2 \cdot \exp(-\|x-x'\|^2/2l^2)$. To validate our model, we establish two types of datasets in the this 1D regression experiment.

First, we set the parameters of the RBF kernel as $s = 3$ and $l = 3$. Hence, as shown in Figure E.3a, all datasets are drawn from continuous and smooth functions. Second, we consider the noisy situations in the first scheme. We intend that the suggested scheme represents the actual real-world situation. Unlike the existing studies [1, 3, 6], we modify the RBF kernel function adding a high frequency periodic kernel function $k(y, y') = s^2 \cdot \exp(-2\sin^2(\pi\|x - x'\|^2/p)l^2)$. Lee et al. (2020) proposed a noisy situation by using random noises sampled by t-distribution; however, these noises often have exaggerated values so that the generated function does not have any tendency and seems to be entire noises. On the other hand, the function generated by Gaussian processes with a high frequent periodic kernel is smooth but is satisfied with a random function every trial. Thus, this function does not interfere with the smoothness of the RBF GP function and maintains the smoothness of all support ranges. Therefore, we decide to use the dataset generated by the RBF GP function with periodic noises to synthetically test all baselines and the proposed method for the robustness of noises. The sampled dataset is graphically presented in Figure E.3b.

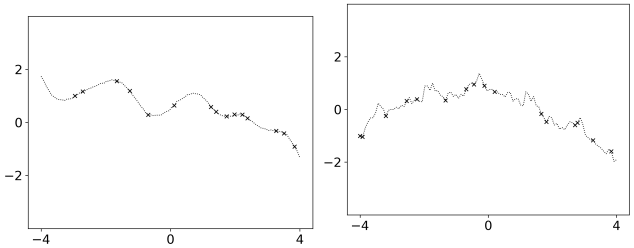

(a) The RBF kernel GP

(b) The RBF kernel GP with periodic noises

Figure E.3: Comaprison of RBF GP functions in 1D regression problems

To generate function values of the Gaussian process, the GPy library[5] provides various functions compatible for PyTorch[6]. In the GPy, $\|x - x'\|^2$ can be regarded as the pre-defined vector $\{1, \ldots, \text{freq}\}^T\{1, \ldots, \text{freq}\}$. We set the parameters of the periodic kernel as freq $= 30$, $p = 2\pi$, $s = 1$. The generated functions for training datasets are shown in Figure E.3.

To test generalization to a novel task, we introduce other functions such as the Matern32 kernel GP and the periodic kernel GP as shown in Lee et al. (2020)[6]. In this experiment, we expect the trained models to capture context points despite different functions. Naturally, all models perform well on the RBF GP function because the meta-training set is generated from RBF GP functions; instead, we test all baselines on other types of functions such as the Matern32 kernel GP and the Periodic kernel GP as well as the RBF kernel GP. For the Matern32 kernel $k(x, x') = s^2(1+\sqrt{3}\|x-x'\|)\exp(-\sqrt{3}\|x-x'\|)$ and the periodic kernel is same as mentioned earlier. The shared parameters of these three GPs are same as $s = 3$, $l = 3$. The periodic kernel requires another parameter freq $= 10$, which is the default value in the GPy.

To elaborate the meta-training framework, the minimum number of context points is 3, and the minimum number of target points is 6, including the context data points. The maximum number of context points and target points is respectively 97 and 100. In the following subsection, we report experimental results, including clean and noisy situations.

[5]https://github.com/SheffieldML/GPy

[6]https://pytorch.org

Table E.4: Results of likelihood values on the synthetic 1D regression without noises. **Bold entries** indicates the best results.

	RBF kernel GP		**Matern kernel GP**		**Periodic kernel GP**	
	context	target	context	target	context	target
CNP	1.136±0.044	0.762±0.090	-0.465±0.106	-3.684±0.222	-2.354±0.218	-9.612±0.0287
NP	0.687±0.030	0.312±0.127	-1.222±0.055	-3.546±0.268	-2.252±0.115	-6.038±0.195
ANP	1.326±0.004	0.819±0.023	0.963±0.039	-1.538±0.083	-0.193±0.219	-7.447±0.278
(Weight decay; $\lambda = 1.0e-3$)						
CNP	1.167±0.025	0.827±0.051	-0.310±0.067	-3.135±0.178	-2.278±0.170	-8.840±0.259
NP	0.695±0.031	0.297±0.051	-1.297±0.201	-3.583±0.536	-2.577±0.223	-6.489±0.268
ANP	1.355±0.002	0.924±0.035	1.077±0.023	-1.753±0.089	0.379±0.080	-7.663±0.325
(Importance Weighted ELBO; $k = 5$)						
CNP	1.170±0.023	0.803±0.083	-0.443±0.130	-3.704±0.296	-2.422±0.151	-9.639±0.330
NP	0.728±0.028	0.255±0.156	-1.476±0.054	-4.208±0.175	-3.042±0.399	-7.463±0.624
ANP	1.344±0.004	0.889±0.037	0.854±0.050	-1.854±0.114	-0.483±0.198	-7.900±0.201
(Bayesian Aggregation)						
CNP	1.282±0.014	0.978±0.019	-0.141±0.140	-3.443±0.294	-2.016±0.168	-9.703±0.221
NP	0.379±0.023	0.069±0.051	-0.751±0.074	-1.811±0.0.066	-1.465±0.092	**-3.308±0.177**
(Regularization for local representation)						
ANP *(dropout)*	1.348±0.001	0.866±0.029	0.902±0.051	-1.753±0.084	-0.520±0.211	-8.052± 0.324
Bootstrapping ANP	1.347±0.005	0.895±0.026	0.790±0.044	-1.834±0.084	-0.983±0.309	-8.463± 0.343
Proposed Method	**1.343±0.006**	**0.937±0.040**	1.170±0.013	**-1.708±0.043**	0.681±0.052	-7.807±0.399

E.1 Experiment Result on RBF GP Functions

We train all baselines on the RBF GP functions without noises. We demonstrate experimental results in terms of predictability and context set encoding.

As shown in Table E.4, all models are capable of fitting the RBF GP function; meanwhile, all models are degraded in cases of Matern kernel GP and Periodic GP. Unlike all baseline models, of which performances drop substantially, the proposed method has relatively small degradation. Particularly, the proposed method records that the likelihood value of context points at Matern kernel GP and Periodic GP is respectively 1.170 and 0.680. Meanwhile, the best performance among baselines is 1.077 and 0.379 by ANP with weight decay. This result shows that the proposed method performs better than all baselines. The graphical results are described in Figure E.4.

E.2 Experiment Result on RBF GP Functions with Noises

As mentioned early in the current section, we train all models on the RBF GP functions adding the random periodic noise. Looking at the column of RBF kernel GP in Table 1, most of the baselines are degraded due to noisy situations. However, the performances of all baselines are improved in Matern GP and Periodic GP. We guess that this phenomenon can be explained as mitigating memorization issues by injecting random noise to the target value [29]. We present how effectively random noises improve generalization performances for all baselines and our method in this experiment. However, we can recognize that injecting random noises cannot be a fundamental solution. As seen in Appendix G, we emphasize that capturing and appropriately utilizing context information when predicting target values is a fundamental solution to avoid memorization in a given situation. The experimental result is described in Table 1 on manuscript and the detailed graphical explanation is suggested in Figure E.5.

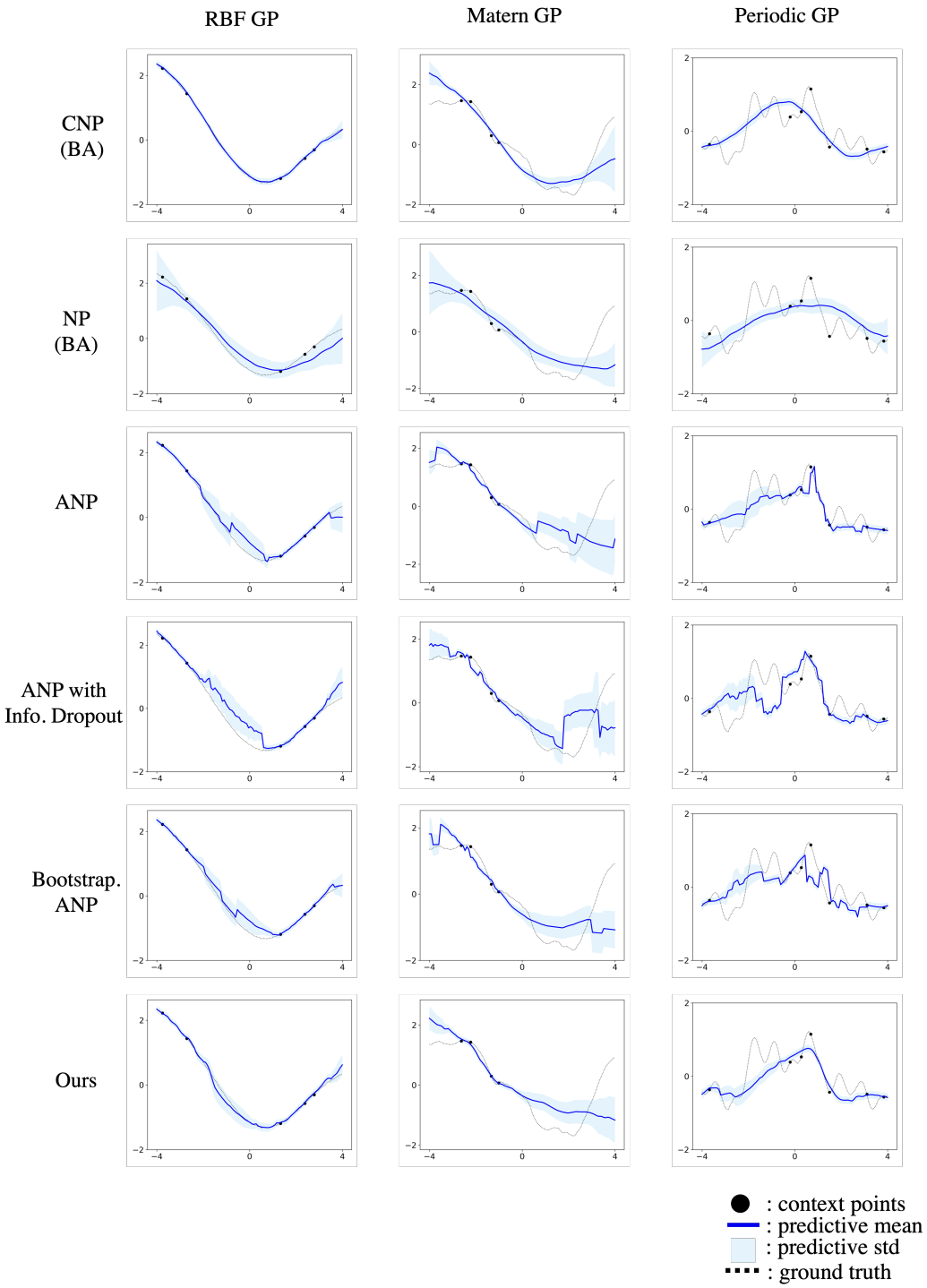

Figure E.4: 1D regression results by NPs trained on the RBF kernel function without periodic noises. All baselines and ours fit the RBF GP function, but degrade their performances in cases of Matern and Periodic kernel GP.

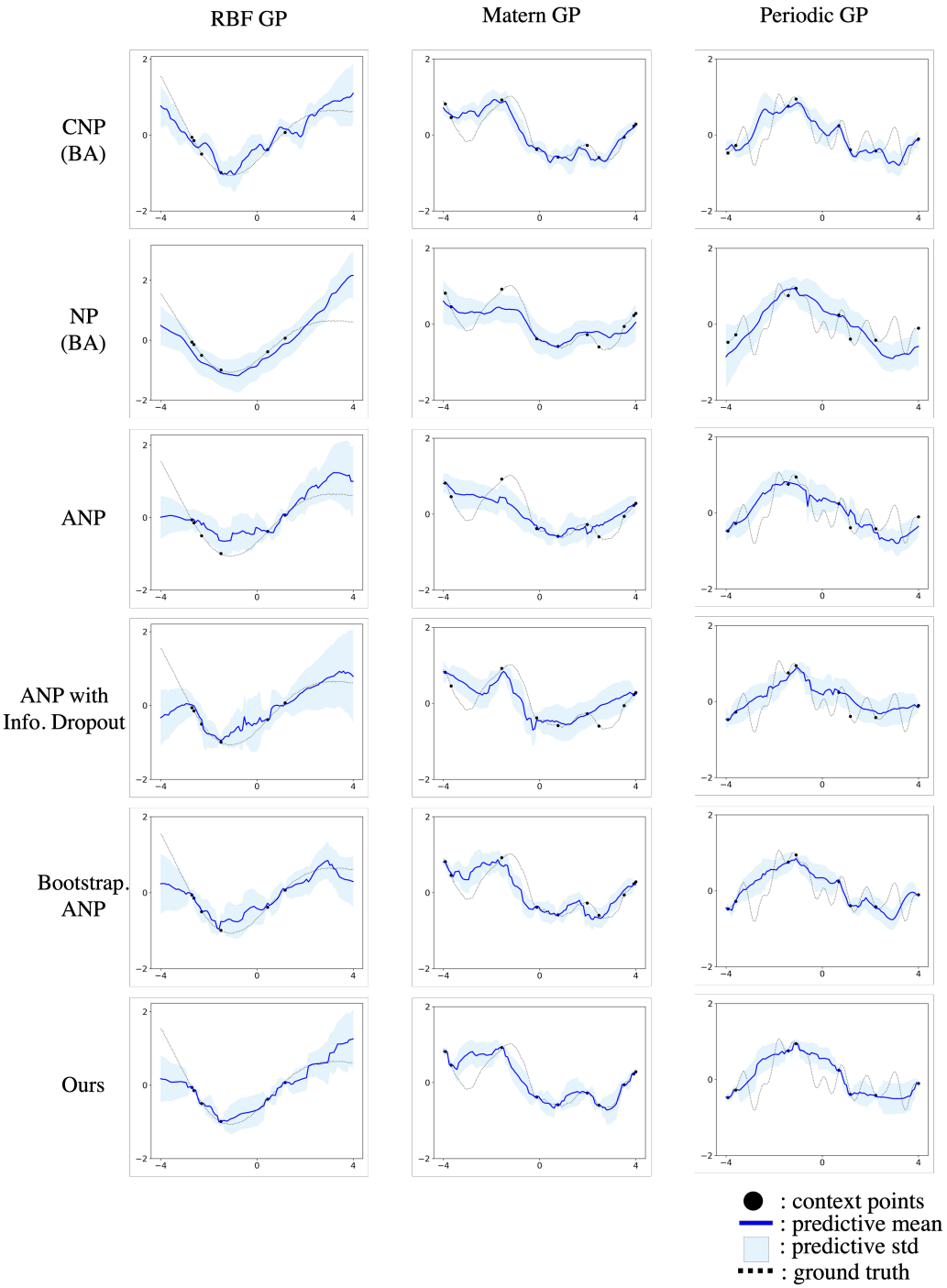

Figure E.5: 1D regression results by NPs trained on the RBF kernel function with periodic noises. All models improve performance in Matern and Periodic GP than Figure E.4. The proposed method outperforms baselines and regularization methods. Even this model achieves better performance than the result on RBF GP without noises.

F Predator Prey Model

We follow the experimental detail in this paper [6, 9]. This experiment is designed to evaluate all baselines capable of adapting new tasks, which have slightly different task distributions. It is called "Sim2Real". We assume that, in this situation, we easily obtain simulation data, but it requires a high expense to collect real-world data points. We try to train all baselines on the dataset generated by simulations and test them on real data sets that are relatively small compared to the simulation data.

The way of simulated data is generated from the Lotka-Volterra model(LV model) [30]. Note that X is the number of predators, and Y is the number of prey at any time step in our simulation. According to the explanation, one of the following four events should occur. The following events require the parameter $\theta_1 = 0.01, \theta_2 = 0.5, \theta_3 = 1, \theta_4 = 0.01$

1. A single predator is born according to rate $\theta_1 \cdot X \cdot Y$, increasing X by one.
2. A single predator dies according to rate $\theta_2 \cdot X$, decreasing X by one.
3. A single prey is born according to rate $\theta_3 \cdot Y$, decreasing Y by one.
4. A single prey dies(or is eaten) according to rate $\theta_4 \cdot X \cdot Y$, decreasing Y by one.

The initial X and Y are randomly chosen. On the other hand, Hudson's bay lynx-hare dataset follows a similar tendency to the LV model; however, it is oscillating time series because it has been collected in real-world records. There were unexpected outliers, unexplained events, and noise. For the detailed explanation, refer gordon et al. (2019)'s work [9]. All simulation codes are available on this URL[7]. The generated simulation data can be graphically shown as the left side of Figure F.6.

In this experiment, we set $d_x = 1$, $d_y = 2$, and all remaining settings are the same as the 1D regression experiment except that the number of context points is at least 15 and the extra target points is also at least 15. When training models, we use the dataset generated by the LV model and test on the lynx-hare dataset. The experimental result is shown in Table 2, and the prediction performance can be graphically shown in Figure F.6.

We conduct additional experiments to validate whether the random periodic noise positively influences the performance. As conducted in the 1D regression experiment, we utilize the periodic kernel GP function, which has very high frequency freq $= 100$ to add noises to the training dataset. As shown in Table F.5 compared to Table 2, We recognize that adding random periodic noise empirically improves all baselines and our method. Among models, our models perform best due to the full representation of context and target datasets. The prediction results can be graphically shown in Figure F.6b

Table F.5: Predator-prey model results. All models are trained on data with periodic noises.

	Simulation		**Real data**	
	context	target	context	target
CNP	-0.181	-0.308	-2.420	-2.789
NP	-0.641	-0.739	-2.464	-2.710
ANP	0.645	0.290	-0.634	-1.962
(Importance weighted ELBO ($s = 5$))				
CNP	-0.284	-0.390	-2.484	-2.864
NP	-0.527	-0.628	-2.335	-2.641
(Bayesian Aggregation)				
CNP	-0.060	-0.171	-2.393	-2.776
NP	-0.357	-0.458	-2.260	-2.618
(Regularization for local representation)				
ANP *(information dropout)*	-0.749	-0.990	-1.766	-2.458
Bootstrapping ANP	0.326	-0.008	-1.183	-2.008
Ours	**2.745**	**1.819**	**2.699**	**-0.076**

[7] https://github.com/juho-lee/bnp

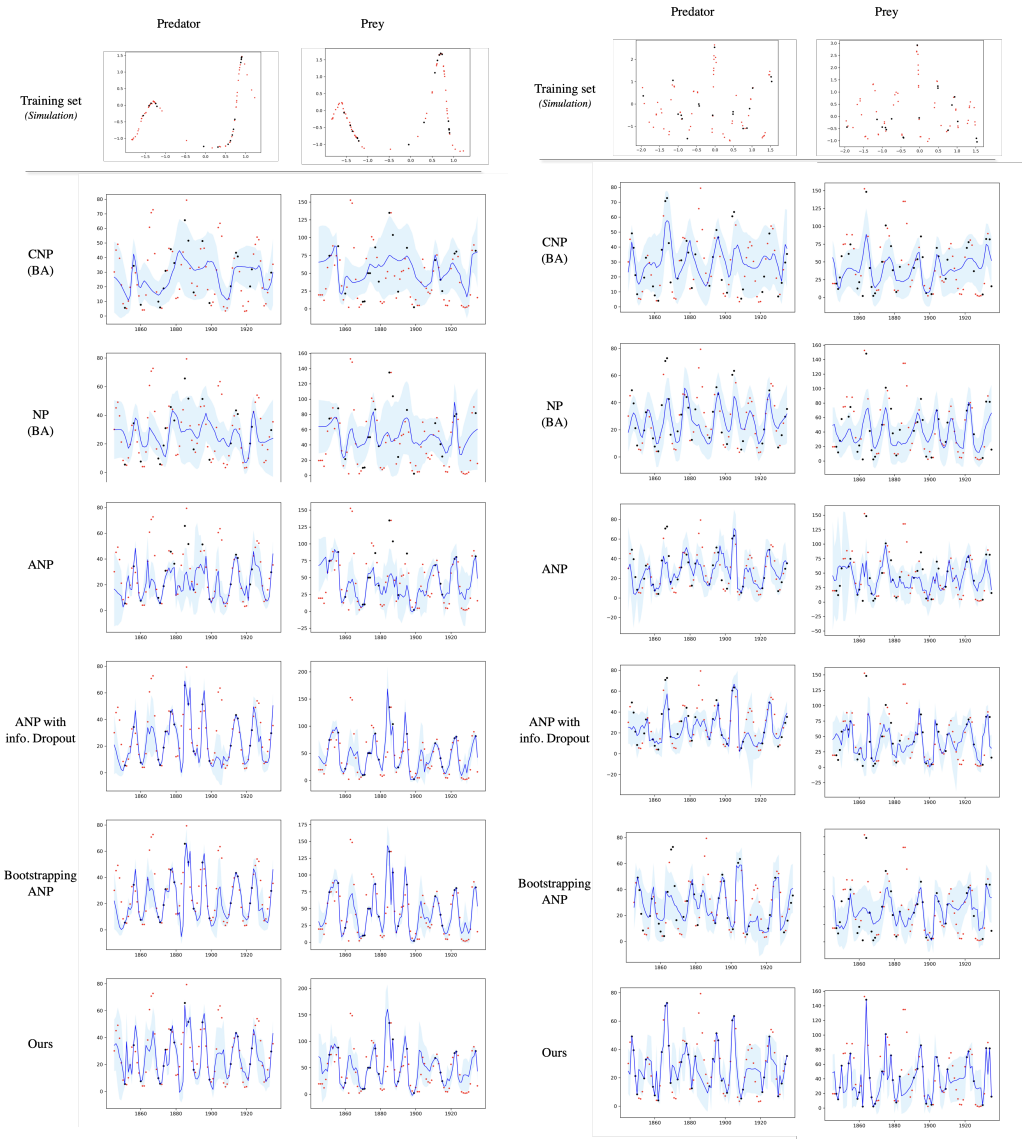

(a) On the clean data

(b) On the noisy dataset.

Figure F.6: Prediction results on the hare-lynx data. (*left*) All models are trained on the clean dataset. (*right*) All models are trained on the noisy dataset.

G Anlaysis of Context Embeddings via Attention Weights in 1D Regressions and the Lynx-hare Dataset

The attention mechanism can explicitly display the distance between context and target data points via attention weights. Especially, when the dimension of features is one, $x \in \mathbb{R}^1$, the distance between features is simply calculated and sorted, so allowing for straightforward comprehension when the attention weights are shown in heat-maps. As a result, we present several heatmaps to compare ours with baselines in both clean and noisy 1D regression datasets. The horizontal axis in these graphs represents the value of features in the context dataset, while the vertical axis represents the value of features in the target dataset. The best pattern for this heat-map is diagonal because all feature values are arranged in ascending order. Additionally, we will provide the simplified heat-map that take into account only target points with same value in the context dataset. Due to the fact that the original version has one-hundred target points, labels and ticks are necessarily small. We guess that readers may be unable to decipher the detailed information such as labels and attention scores. This simplified version allows the readers to instantly grasp what we attempt to convey by exhibiting a more distinct diagonal pattern. From Figure G.7 to Figure G.9, on the left side, we show a simplified version of the attention score; on the right side, we show the result for the entire target dataset. Plus, we provide Sim2Real's attention heat-maps in both clean and noisy environments. As a result, our discovery appears to be consistent.

First, the heatmaps of the 1D regression problem without perioidc noises are shown in Figure G.7. In this graph, all models including ours can accurately depict the similarity between the context and targete dataset. Although the attention scores for each model vary, it is clear that the majority pattern of all models is diagonal. Therefore, all models are trained using the clean dataset in the intended manner. However, other phenomena are found in the noisy data. We identify that the attentive neural process [3] fails to capture contextual embeddings because the attention weights of all target points highlight on the lowest value or the maximum value in the context dataset. In the case of the Bootstrapping ANP [6] and ANP with information dropout, the quality of heat-map is slightly improved, but it still falls short of ours. This indicates that the present NPs are unable to properly exploit context embeddings because the noisy situations impair the learning of the context embeddings during meta-training. On the other hands, even in the noisy situation, the attention score in ours still appear clearly. Second, we include heatmaps for the Sim2Real problem. As seen in Figure F.6, the context and target datapoints are much too many for the label information and ticks to be recognized. Hence, we recommend that readers verify the presence of diagonal patterns rather than examining detailed numerical values. As seen in Figure G.9a, all models are capable of capturing properly similarity between the context and target datasets. However, as with 1D regression, the diagonal pattern of the baselines is disrupted as seen in the left graph of Figure G.9b; nevertheless, ours retains the ideal pattern in both clean and noisy situations.

When comparing our model's heat-map pattern in clean and noisy environments, there is a noteworthy point. Our model is capable of learning adaptively how to focus on certain context datapoints depending on the extent of dirty data in the meta-train dataset. The model is trained on the clean dataset to take into consideration nearby points as well as the corresponding point in the context dataset, hence, the heat-map gradually changes. This is because the clean dataset has smooth values, $y_{i,j}$, near a certain feature $x_{i,j}$. Meanwhile, in the noisy dataset, the model is trained to focus exclusively on corresponding points to the context dataset. Hence, the heat-map in Fig E.5 (b) indicates that attention score of target datapoints that includes the context dataset has a high value, whilst the remainder points treat all context datapoints uniformly. This phenomena occurs because there is less correlation between adjacent features $x_{i,j}$ and its labels $y_{i,j}$ in the noisy situation during the meta-training.

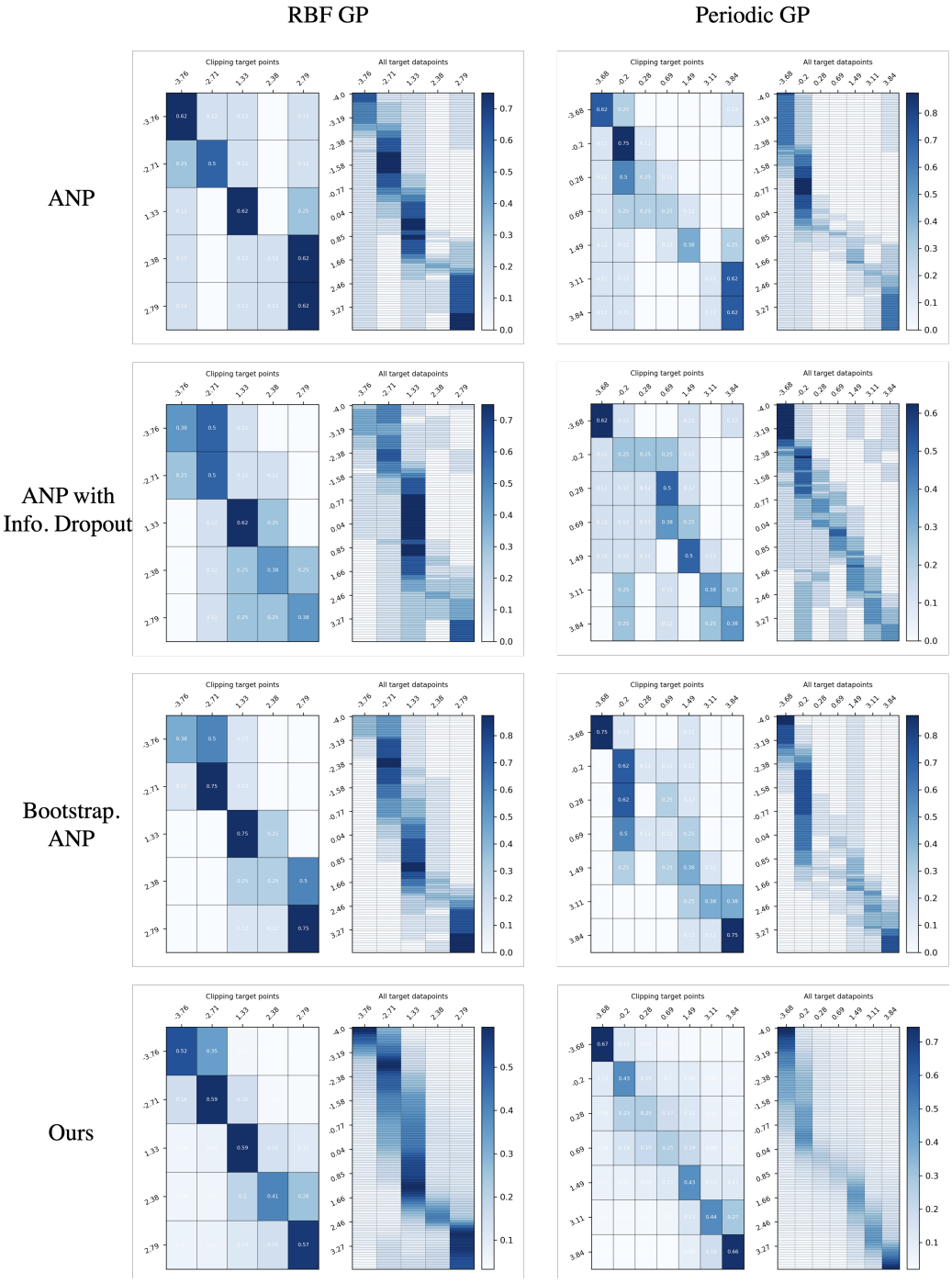

Figure G.7: Heatmaps of asscociated attention weights in 1D regression problems when test datasets are sampled from RBF and Periodic kernel functions. All models are trained on the clean dataset. (*Left*) A simplified heat-map that takes into account only target datapoints with same value in the context dataset. (*Right*) A heat-map that takes into account entire target datapoints.

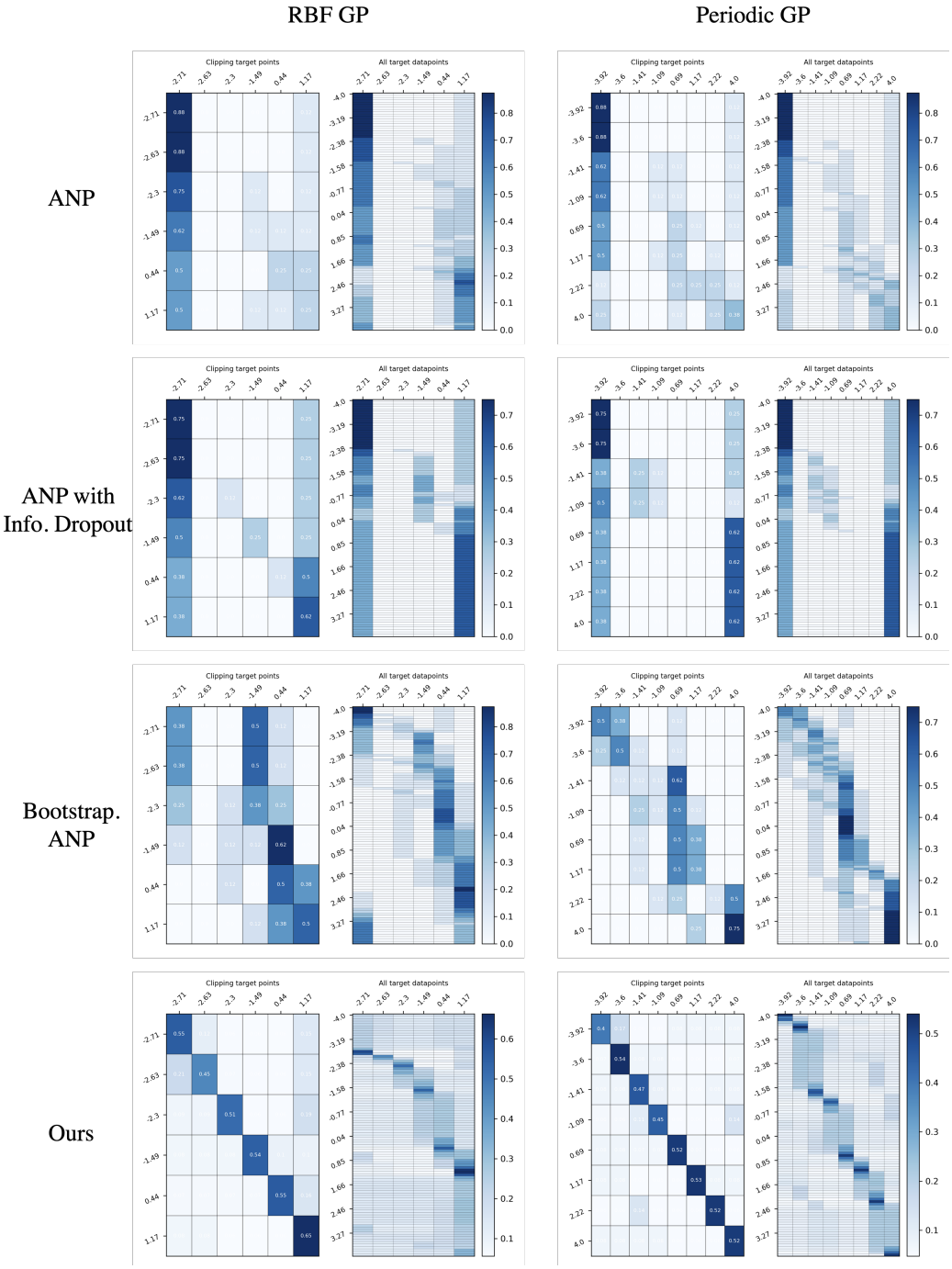

Figure G.8: Heatmaps of asscociated attention weights in 1D regression problems when test datasets are sampled from RBF and Periodic kernel functions. All models are trained on the data with periodic noises. (*Left*) A simplified heat-map that takes into account only target datapoints with same value in the context dataset. (*Right*) A heat-map that takes into account entire target datapoints.

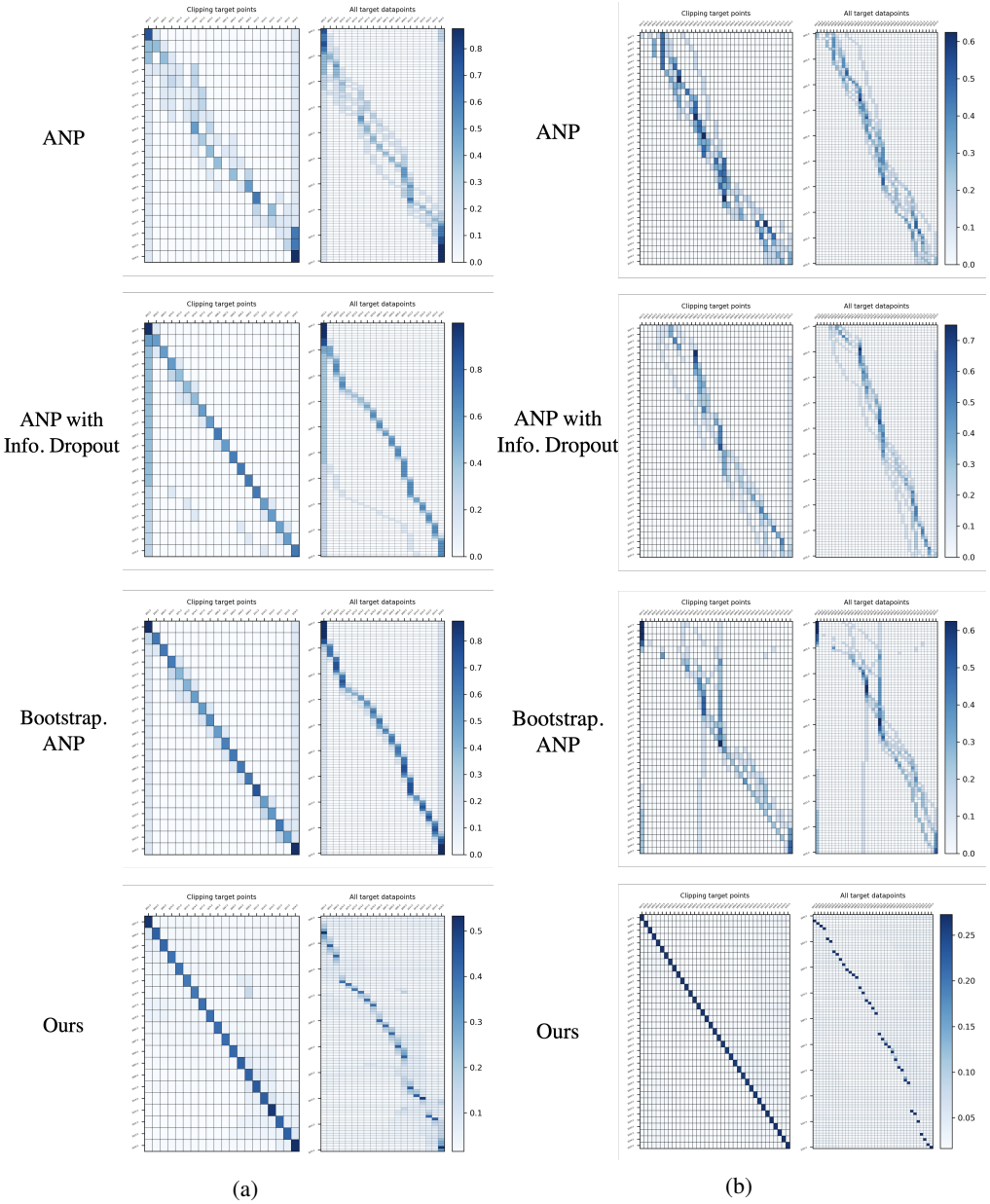

Figure G.9: Heatmaps of asscociated attention weights in the hare-lynx dataset. (*Left*) A simplified heat-map that takes into account only target datapoints with same value in the context dataset. (*Right*) A heat-map that takes into account entire target datapoints. (a) All models are trained on the clean dataset by the lotka-volterra simulation (b) All models are trained on the lotka-volterra simulation with periodic noises.

H Movielenz-100k data

We follow the experimental detail in the paper [31]. The way to split into train, test, validation dataset is described in this work[8]. Briefly, all ratings are first divided into two datasets, which respectively have user IDs and are not duplicated each other. We define that one is the meta-training dataset and the other is the meta-test dataset. In this experiment, we evaluate baselines that generalize to a new customer with small history data points. To explain a training regime, the number of context is at least three and the objective function is computed with the remaining data points. All users do not have the same amount of ratings so that the number of data points is varying during meta-training. When testing baselines, we sample a few ratings from unobserved users and then evaluate the likelihood values for the remaining points. To exclude users' unique information, we drop the User ID from the set of features and only use general features such as age, occupation. Lastly, in this experiment, we set $d_x = 44$, $d_y = 1$, and all remaining settings are the same as the 1D regression experiment. The detailed explanation is in galashov et al. (2019)'s work [31]. The likelihood values on the MovieLens-10k is reported in Table H.6.

Table H.6: Results of likelihood values on the MovieLens-10k. **Bold entries** indicates the best results.

	context	**Target**
CNP	-24.718	-23.908
NP	-23.096	-22.135
ANP	-1.456	-2.042
(Weight decay; $\lambda = 0.001$)		
CNP	-23.524	-23.098
NP	-15.876	-16.109
ANP	-0.891	-1.865
(Importance Weighted ELBO; $s = 5$)		
CNP	-17.276	-17.799
NP	-25.322	-25.233
ANP	-17.205	-16.427
(Bayesian Aggregation)		
CNP	-12.472	-12.141
NP	-11.911	-11.859
(Regularization for local representation)		
ANP *(dropout)*	-1.742	-2.434
Bootstrapping ANP	-16.267	-16.191
Ours	**-0.349**	**-1.617**

To compare RMSE scores with existing methods for Movielens-100k data, we suggest evaluating NPs using u1.base and u1.test. As mentioned, the prediction by NPs is based on given context data points. First, we randomly choose a customer in the u1.test. Second, we randomly sample a small number of ratings from u1.base, which is used as the meta-training data. In this experiment, we decided to draw ten samples from u1.base and employ these points as the context data set. The ten ratings is relatively a short history compared to the size of the u1.base. Third, we perform predictions for the data points in the u1.test based on the context data points. The important thing is that context and target data points are sampled from the same user but the different data set. Plus, we do not touch in information in the test set, at least. Based on the relationship between sampled context points and target points, the performance of NPs is somewhat variable, so we report five runs and average these results. The experimental result is in Table 3.

[8] https://tinyurl.com/yyfzlg2x

I Image Completion

In the image completion task, we follow the training regime suggested by NPs [1, 2]. In this regime, d_x means the pixel location and d_y means the color RGB data. Namely, we set $d_x = 2$ and $d_y = 3$. For high capacity representation, the dimension of all hidden units is determined as $d_h = 512$. All remaining settings, including layer sizes, are the same as the 1D regression experiments.

When it comes to image completion tasks, according to these papers, NPs are known to complete facial images given partial pixels. Although a few pixels are provided, NPs are capable of understanding the common appearance of a human face. These models generate eye, mouth, and nose even if only a small number of local information is given, which is generally hard to recognize. The Conditional neural process properly performs; however, it often loses its context representations. The Attentive neural process tackles this issue to employ an attention mechanism. Instead of the encoders consisting of MLP layers, the self-attention can improve the quality of pixels generated at the context data points. However, as mentioned on subsection 4.2, scores of generated pixels in unseen regions are still problems. Even though many pixels are provided, the quality of completed images is not improved. In this work, the proposed method concentrates on given contextual pixels and complete images based on that information. Hence, the proposed method completes an image with high uncertainty when few pixels are given. Plus, it can be seen that the higher the pixels information, the higher the quality of generated images. The numerical result is presented in Table 2, the graphical evidences are shown in from Figure I.10 to Figure I.13.

The proposed method allows for completion of images using only partially provided pixels, so it enables to complete larget images than the image size in the training dataset. We produce images of various sizes using the proposed method, which is trained on the CelebA dataset with size of 32×32. The completed images are presented in Figure I.14. When we qualitatively evaluate the completion results, the proposed method properly perform for generating large images without sacrificing performance. All completed images are quite close to the ground truth. As a result, we conclude that the proposed method can be used for *task adaptation* since it can complete images that the model have never encountered during meta-training and whose sizes differ from the training dataset. In particular, while the percentage of contributed pixels to the total number of pixels remains constant, the quality of completed images are enhanced according to the amount of provided pixels. We understand that the number of pixels is more significant than the ratio of context points. This is because the model has a sufficient pixel counts to work with when images are large. For instance, employing only 300 pixels as a context dataset is insufficient to complete the images. Nonetheless, the completed images with 300 pixels are comparable to those with higher pixel counts and is of higher quality than the baselines in Figure I.12.

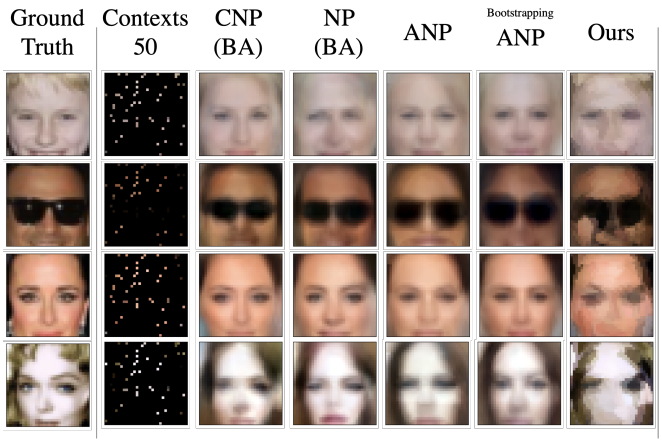

Figure I.10: Completed images using 50 pixels

There is an interesting discovery of uncertainty values in the image completion task. Basically, we expect that many pixels reduce the uncertainty of generated images. However, the existing methods stably generate facial images, but uncertainty values do not decrease even if available pixels increase. The proposed method makes high variance for a completed image under the small number of context

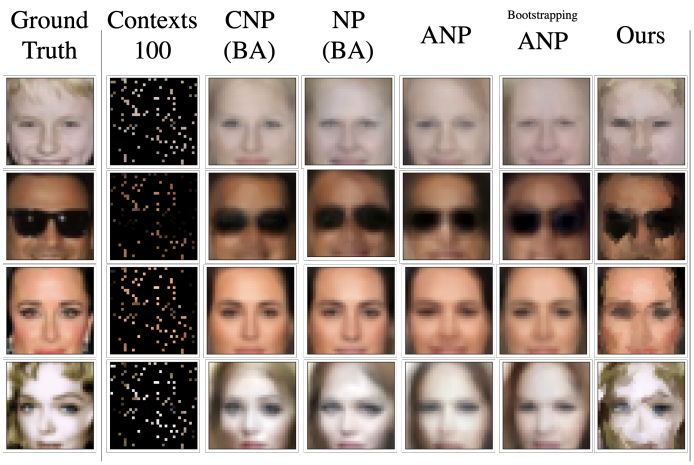

Figure I.11: Completed images using 100 pixels

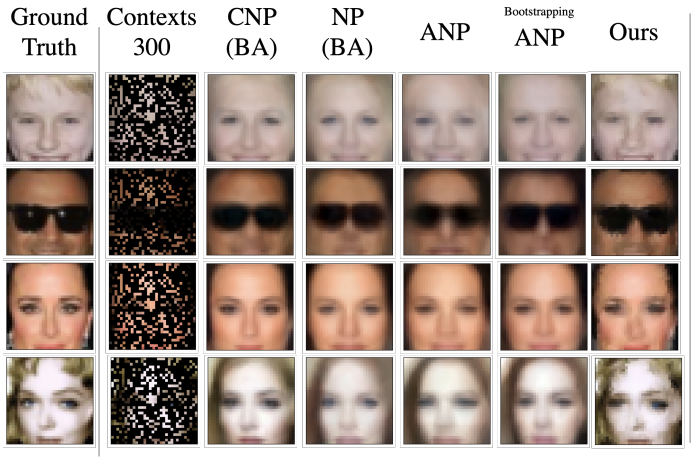

Figure I.12: Completed images using 300 pixels

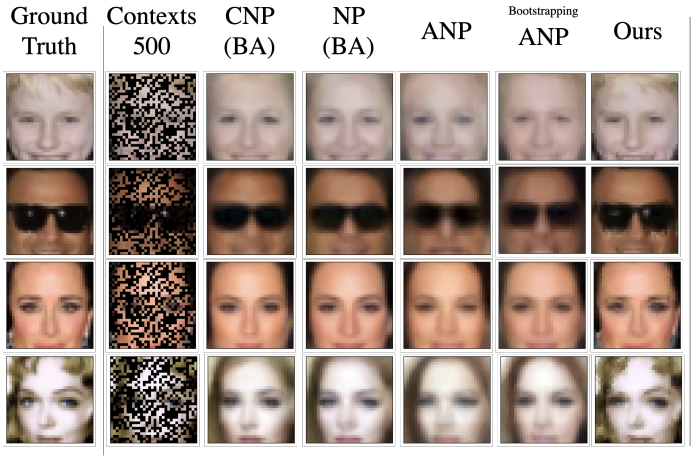

Figure I.13: Completed images using 500 pixels

points. As shown in Figure I.15, it can decrease the uncertainty of completed images when the

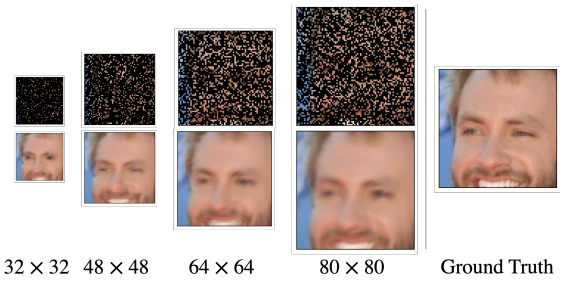

(a) Example 1

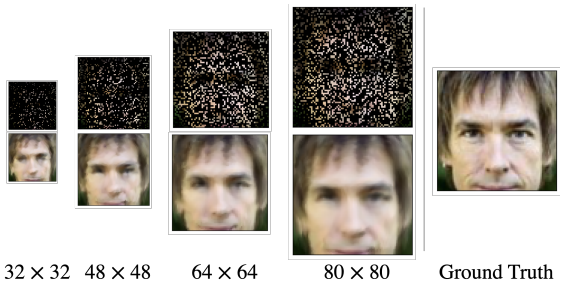

(b) Example 2

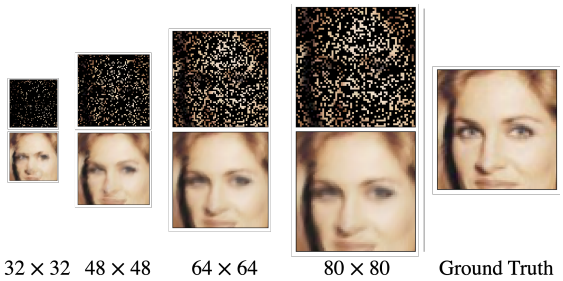

(c) Example 3

Figure I.14: Our completed images in a variety of sizes. The training dataset consists of the CelebA images with a size of 32×32. The completed images range in size from 32×32 to 80×80. Each image is completed with 0.3 of the overall pixels. As the image size increases, the following values are used as the number of context points;$\{300, 690, 1230, 1920\}$. Both the context dataset and its completed image are displayed. Additionally the most right column has the ground truth image. Each image is shown in proportion to its image size.

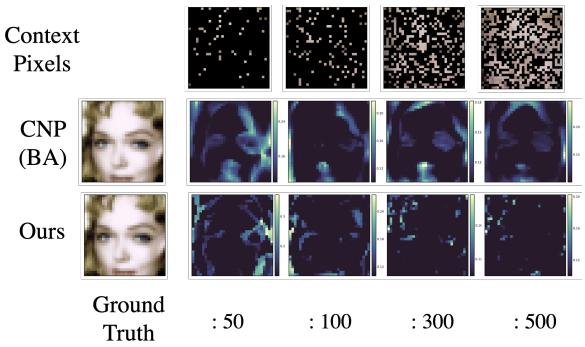

Figure I.15: Comparison of quality of uncertainty by CNP with Bayesian aggregation and Ours.

number of context points is large. From this fact, we identify that the proposed method performs in an intended manner.